J Mol Model (2013) 19:4969–4989
DOI 10.1007/s00894-013-1998-2

ORIGINAL PAPER

Destabilization of the MutSα's protein-protein interface due to binding to the DNA adduct induced by anticancer agent carboplatin via molecular dynamics simulations

Lacramioara Negureanu · Freddie R. Salsbury Jr

Received: 1 July 2013 / Accepted: 5 September 2013 / Published online: 24 September 2013

Abstract DNA mismatch repair (MMR) proteins maintain genetic integrity in all organisms by recognizing and repairing DNA errors. Such alteration of hereditary information can lead to various diseases, including cancer. Besides their role in DNA repair, MMR proteins detect and initiate cellular responses to certain type of DNA damage. Its response to the damaged DNA has made the human MMR pathway a useful target for anticancer agents such as carboplatin. This study indicates that strong, specific interactions at the interface of MutSα in response to the mismatched DNA recognition are replaced by weak, non-specific interactions in response to the damaged DNA recognition. Data suggest a severe impairment of the dimerization of MutSα in response to the damaged DNA recognition. While the core of MutSα is preserved in response to the damaged DNA recognition, the loss of contact surface and the rearrangement of contacts at the protein interface suggest a different packing in response to the damaged DNA recognition. Coupled in response to the mismatched DNA recognition, interaction energies, hydrogen bonds, salt bridges, and solvent accessible surface areas at the interface of MutSα and within the subunits are uncoupled or asynchronously coupled in response to the damaged DNA recognition. These pieces of evidence suggest that the loss of a synchronous mode of response in the MutSα's surveillance for DNA errors would possibly be one of the mechanism(s) of signaling the MMR-dependent programed cell death much wanted in anticancer therapies. The analysis was drawn from dynamics simulations.

Keywords MD simulations · Mismatch repair proteins · MMR · Platinum-DNA adducts carboplatin-induced damage DNA recognition · Protein-protein interface destabilization

Introduction

DNA mismatch repair (MMR) proteins maintain genetic integrity in virtually all organisms [1] by recognizing and repairing post-replicative DNA errors [2]. Such alteration of hereditary information can lead to various diseases, including cancer, and defective MMR genes are associated with increased risk of cancer [3]. Besides their role in DNA repair during the cell division, the system of MMR proteins also detect certain types of DNA damage, initiating cellular death responses [4, 5], making the proteins in MMR pathway, particularly the human recognition protein complex MutSα (Msh2-Msh6), potential targets for the development of anticancer agents [5–7].

A highly conserved process from prokaryotes to eukaryotes, the DNA repair in eukaryotes is initiated by the concerted action of several MMR complexes, namely MutSα, MutSβ (Msh2-Msh3), and MutLα (Mlh1-Pms2) [2]. In the first step, MutSα heterodimer detects and signals mispaired DNA nucleotides or small insertion/deletion loops. These events lead to MutLα nicking the DNA strand in the vicinity of the error [8]. Subsequently, the nicked strand is excised and the replication machinery resynthesizes DNA. The final cellular outcome is DNA repair [8]. MutSβ heterodimer binds to post-replicative DNA containing insertion/deletion loops of two, three, four or six unpaired nucleotides [9]. A recent study [10]

Electronic supplementary material The online version of this article (doi:10.1007/s00894-013-1998-2) contains supplementary material, which is available to authorized users.

L. Negureanu · F. R. Salsbury Jr (✉)
Department of Physics, Wake Forest University, Winston Salem, NC 27106, USA
e-mail: salsbufr@wfu.edu

indicates large conformational changes in MutS (the *E. Coli* homologue of human MutSα) during DNA scanning, mismatch recognition and repair signaling. The same study also indicates that the life-time of the MutS-DNA complex, in which presumably the protein interacts with downstream proteins required for repair, is on the scale of seconds.

In addition to the DNA repair function, MutSα also recognizes and initiates cellular response to certain types of DNA damage, such as DNA adducts induced by platinum-based anticancer agents [11, 12]. In this case, the final cellular outcome is cell death. The mechanism by which lesion recognition triggers cell cycle checkpoints and apoptosis is not yet resolved [13, 14]. However, it has been established that MMR-dependent DNA repair is uncoupled from MMR damage response to the anticancer agent cisplatin [15].

Carboplatin (*cis*-diammine(cyclobutane-1,1-dicarboxylato)-platinum(II) [16] and its predecessor, cisplatin (*cis*-diammminechloroplatinum(II) [17], are platinum-based anticancer agents used in the treatment of many solid cancers [18]. Since its discovery in 1960's, thousands of platinum analogues have been synthesized and screened for anticancer effect in an attempt to overcome cisplatin's limitations, many have entered clinical trials, but, besides carboplatin, only one other, oxaliplatin, gained international marketing approval [18]. Platinum-based anticancer drugs exert their anticancer effect through the formation of several types of adducts with nuclear DNA [19, 20]. In these adducts the DNA double-helix is severely distorted [21–23]. Sharing the same *cis*-diammine carrier ligands, cisplatin and carboplatin form the same type of platinum-DNA adducts *in vivo*. In these adducts, the platinum atom forms covalent bonds to the N7 positions of imidazole ring of purine bases, primarily guanine, generating 1,2d-(GpGp) and 1,3d-(GpXGp) intra-strand cross-linked adducts, as well as a limited number of inter-strand cross-linked adducts [4]. However, while the 1,2-d(GpGp) intra-strand platinum-DNA adduct is the major component induced by cisplatin [22], the 1,3-d(GpXGp) intra-strand platinum-DNA adduct is considered responsible for the biological activity of carboplatin [22].

Current knowledge on the cellular recognition of the platinum-DNA adducts is based mostly on the cisplatin-induced adducts [4, 6, 24, 25]. Previous studies in our group provided computational evidence suggesting that MutSα proteins recognize mismatched and damaged DNA substrates in significantly different modes [26], and that MutSα signals the mismatched and damaged DNA recognition through independent pathways [27]. These observations are in agreement with experimental evidence indicating that repair-deficient MMR mutants are functional in MMR-dependent cisplatin cytotoxicity [5]. Additionally, Msh2 subunit is indicated "to assist" [26] the mismatch recognition subunit Msh6 in recognition and to play a key role in signaling both mismatched and damaged DNA recognition [27].

The focus of this study is on conformational and structural changes at the protein-protein interface of MutSα complex in response to carboplatin-induced damaged DNA recognition, as derived from atomistic molecular dynamics simulations of the MutSα-DNA recognition complex. Nonbonding interactions energies, solvent accessible surface area, contact maps, hydrogen bonding, and salt bridges calculations at the protein-protein interface in the carboplatin-damaged complex will be contrasted to those found in the mismatched DNA recognition complex.

These data indicate that strong, specific interactions at the MutSα's protein-protein interface in response to the mismatched DNA recognition are replaced by weak, non-specific interactions in response to the damaged DNA recognition, suggesting a severe impairment of the dimerization of MutSα in response to the damaged DNA recognition. While the core of MutSα is preserved in response to damaged DNA recognition, the loss of contact surface and the rearrangement of contacts at the protein-protein interface suggest a different packing in response to damaged DNA recognition. Coupled in response to the mismatched DNA recognition, interaction energies, hydrogen bonds, salt bridges, and solvent accessible surface area at the interface of MutSα and within subunits are uncoupled or asynchronously coupled in response to the damaged DNA recognition.

These pieces of evidence suggest that the loss of a synchronous mode of response while "surveying" post-replicative DNA errors would possibly be one of the mechanism(s) of signaling the MMR-dependent programed cell death much wanted in anticancer therapies. Such knowledge would advance the understanding of the mechanism of the cellular processing of the damaged DNA by MMR pathway.

The results at the MutSα's protein-protein interface in the carboplatin-induced damaged DNA recognition complex are similar to those in the cisplatin-induced damaged DNA recognition complex, and the latter system has been the subject of multiple computational studies with experimental validation in our group [5, 7]. Specifically, employing the same simulation protocol, 2–10 ns of simulations of the *E. Coli* homologue (MutS) molecular complex have been experimentally verified to be sufficient to examine the experimental questions addressed in the MutSα mismatched and cisplatinated DNA complexes [5, 6, 15]. To this end, changes associated with the DNA damage response, such as conformational differences in disordered loops at the protein-protein interface, conformational changes associated with ATP binding/hydrolysis, and key protein-DNA contacts, predicted by conformational analysis of MutS complex with cisplatin-damaged DNA were validated by mutational and genetic analysis experiments [6]. Most importantly, mutational and cell survival studies [6] confirmed that predicted inter-subunit interactions are essential for the repair event and that these inter-subunit interactions are absent or altered in the cisplatin-DNA complex.

Methods

Molecular dynamics simulations

Preparing the MutSα-DNA complex

The structural model for our simulations on 1,3-d(GCG) intra-strand platinum-DNA adduct recognition by the MMR machinery was based on the X-ray structure [28] of human Msh2-Msh6 heterodimer complex with duplex DNA and two ADP molecules bound in the ATPase sites of the heterodimer (PDB ID 2O8B). Each subunit of MutSα is divided into five domains [28]: the mismatch binding domain, the connector domain, the lever domain, the clamp domain, and the ATPase domain (Fig. 1). A complete list of residues sequence and numbering is included in Online resource 1, Figs. 1 and 2.

All protein residues were considered in their default protonation state at physiological pH. Coordination of [*cis*-$Pt(NH_3)_2]^{2+}$ fragment to DNA, in which platinum atom links N7 atoms of two guanines form the same DNA strand, G8 and G10, alters the duplex DNA. The mismatched DNA was used as a template in building the 1,3 intra-strand platinum cross-link. The cross-linked structure was fitted into the binding pocket of the protein to maximize the structural overlap with the mismatched DNA structure, followed by rotations and translations to minimize the energy of the unrelaxed structure using the coordinate manipulation and energy minimization facilities of CHARMM [29]. N-terminal residues 1–361, not resolved in the crystalline structure, were omitted from the simulations. Note that in our system residue 1 of Msh6 corresponds to residue 362 in the solved structure. Hydrogen atoms were added using the *hbuild* facility of CHARMM. The prepared structure was fully solvated in a rectangular box of TIP3P water [30] (33,143 molecules of water) using the VMD package [31], keeping a 10 Å minimum distance between each face of the box and the solute. Na^+ and Cl^- ions were added to neutralize the total charge of the solvated system using the Autoionize plugin from VMD. There are 855 amino acids in Msh2, 974 amino acids in Msh6, 30 nucleotides in the DNA substrate, and two ADP molecules, a total of 30,046 atoms in the protein-DNA complex and 129,533 atoms in the simulated recognition complex.

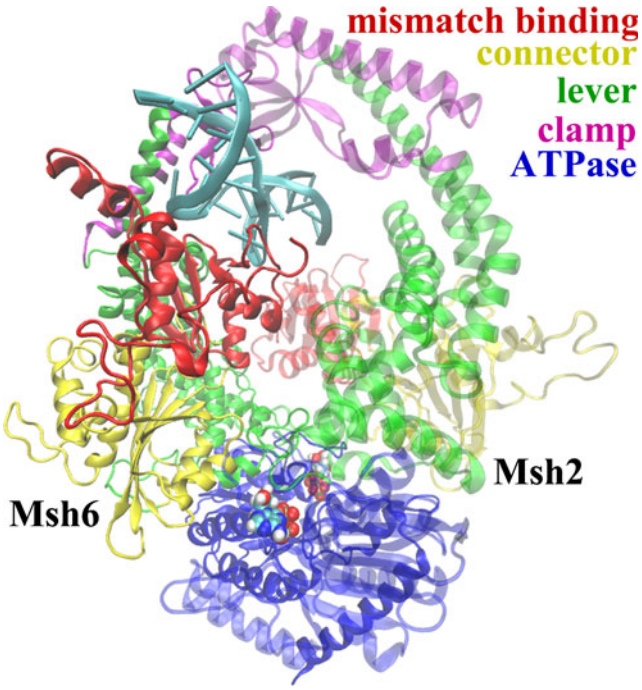

Fig. 1 MutSα-DNA complex structural model DNA is shown in light blue. The color code for the heterodimer domains is as following: red for the mismatch binding domain, residues 1 to 124 in Msh2 and 1 to 157 in Msh6; yellow for the connector domain, residues 125 to 297 in Msh2 and 158 to 356 in Msh6; green for the lever domain, residues 300 to 456 and 554 to 619 in Msh2, and 357 to 573 and 648 to 714 in Msh6; purple for the clamp domain, residues 457 to 553 in Msh2 and 574 to 647 in Msh6; blue for the ATPase domain, residues 620 to 855 in Msh2 and 715 to 974 in Msh6. The two ADP molecules bound to the ATPase domains are depicted in VDW representations. Note that the first 361 residues of Msh6 are unsolved in the X-Ray structure and in our system residue 1 of Msh6 corresponds to residue 362 in the solved structure

Simulations protocol

Simulations were performed using CHARMM27 force field [32] and additional parameters based on preexisting cisplatin parameters [32–34]. CHARMM27 force field has been extensively parameterized for a wide range of biologically important molecules, including amino acids and nucleic acids. Each simulation was the result of a combined CHARMM/NAMD protocol that was derived from earlier protocols [35, 36] that have been used in multiple previous studies [5–7, 26, 27], and the rationale behind it has been reviewed recently [37]. The water molecules were briefly minimized for 100 cycles of conjugate gradient minimization with a small (0.25 kcal/(mol $\cdot Å^2$)) harmonic force constant on all protein atoms. The entire system then underwent 250 ps of molecular dynamics simulation to achieve a thermal equilibration using Berendsen pressure regulation with isotropic position scaling [38]. During the thermal equilibration, the system's temperature was equilibrated by reassigning atom velocities from a Boltzman distribution for a given temperature every 1000 steps, in a 25 K increment, from an initial temperature of 0 K to a target temperature of 300 K Then periodic adjustments of velocities were allowed, if necessary, within the first 125,000 steps.

Following the equilibration, for each simulation, a 20 ns NPT production simulation at 300 K and 1 bar was performed using NAMD package [39] with standard parameters and periodic boundary conditions. All bonds involving hydrogen atoms in the protein were constrained using SHAKE constraint algorithm [40]. A 2 fs integration time step was used

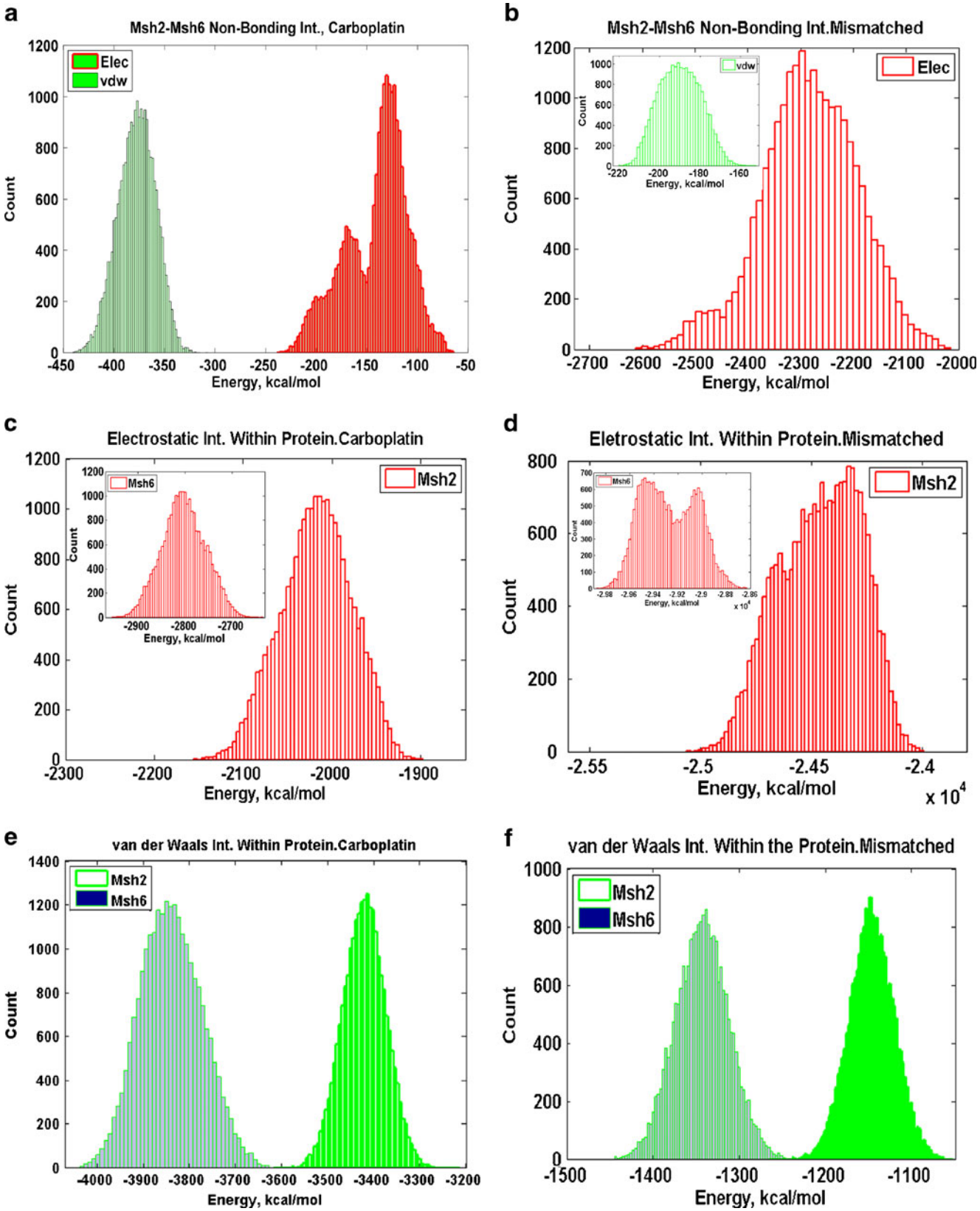
a
Msh2-Msh6 Non-Bonding Int., Carboplatin
Elec
vdw
Count
Energy, kcal/mol
b
Msh2-Msh6 Non-Bonding Int.Mismatched
Elec
vdw
Count
Energy, kcal/mol
c
Electrostatic Int. Within Protein.Carboplatin
Msh2
Msh6
Count
Energy, kcal/mol
d
Eletrostatic Int. Within Protein.Mismatched
Msh2
Msh6
Count
Energy, kcal/mol
x 10^4
e
van der Waals Int. Within Protein.Carboplatin
Msh2
Msh6
Count
Energy, kcal/mol
f
van der Waals Int. Within the Protein.Mismatched
Msh2
Msh6
Count
Energy, kcal/mol

◀ **Fig. 2** Nonbonding interactions histograms for the representative ensemble of structures are presented. Carboplatin-damaged DNA MutSα recognition complex (**a**–**c**). At both Msh2-Msh6 interface and within subunits van der Waals interactions are stronger than electrostatic interactions. At Msh2-Msh6 interface (**a**) van der Waals interactions, −377.59(18.49) kcal mol^{-1}, are stronger than the electrostatics interactions, −140.68(30.97) kcal mol^{-1}. Within the subunits, van der Waals interactions are stronger than electrostatics interactions, and about 400 kcal mol^{-1} stronger within Msh6 than within Msh2, −3839.6(67.25) kcal mol^{-1} versus −3422.21(46.63) kcal mol^{-1} (in **c**). Electrostatic interactions within Msh6 are about 800 kcal mol^{-1} stronger than within Msh2, in (**b**) −2802.50(46.06) kcal mol^{-1} versus −2017.51(39.74) kcal mol^{-1}. Mismatched DNA MutSα recognition complex (**d**–**f**). Unlike in the damage recognition complex, in the mismatch recognition complex at both Msh2-Msh6 interface and within subunits the electrostatic interactions are dominant. At Msh2-Msh6 interface (**d**) electrostatic interactions are dominant over van der Waals interactions, −2282.50(91.61) kcal mol^{-1} versus −189.85(10.26) kcal mol^{-1}. Within subunits electrostatic interactions (**e**) are dominant and about 500 kcal mol^{-1} stronger within Msh6, −29272.00(224.38) kcal mol^{-1}, than within Msh2, −24440.00(147.61) kcal mol^{-1}. van der Waals interactions (**f**) within Msh6, −1343.80(31.30) kcal mol^{-1}, are slightly stronger than within Msh2, −1147.50(26.31) kcal mol^{-1}. Data presented are mean(std)

for all interactions. The van der Waals potential was switched to zero staring at a radius of 8 Å and ending at 12 Å. Particle Mesh Ewald (PME) [41] method for full long-range electrostatics was used, with a maximum space between grid points of 1 Å and a local interaction distance of 12 Å, evaluated every two time steps. Constant temperature was achieved using Langevin thermostat, as implemented in NAMD [39], with a damping coefficient of 5 ps^{-1}. Berendsen's constant pressure algorithm with a target pressure of 1.01325 bar, a compressibility of 45.7 mbar, a relaxation time of 1 ps, and a pressure frequency of 40 fs provided the pressure control during the simulations.

Four simulations employing the same protocol with different initial velocities and the same coordinates were performed. For the production simulations, initial coordinates, velocities and system dimensions were taken from the final state of the corresponding equilibration simulation.

Cα root-mean-square deviations (RMSD) from the starting structure and total energies are provided in Online resource 1, Fig. 3. These data show that there are two different relaxation timescales, a fast one on the 10–100 s of picosecond timescale, and a slow one on the nanosecond timescale. Data show that most of the relaxation to equilibrium occurs within the first 2 ns, and while there may be additional long-time relaxation, starting the simulations analysis at 8 ns allows for a conservative removal of the majority of the non-equilibration effects. Since our four different simulations started from different initial conditions, it is expected they to show different pathways to equilibration, as well as variation in relaxation. Prior to RMSD calculations the solute was aligned to the initial structure by least-square superimpositions performed to remove translational and rotational movements.

The structural model and the molecular dynamics simulations protocol for the simulations of the 1,2 intra-strand platinum-DNA MutSα complex are presented elsewhere [26, 27]. The structural model, in which platinum atom links N7 atoms of central adjacent guanine bases G8 and G9, was built using the G-T mismatched MutSα-DNA complex [28]. Employing the same protocol, the 50 ns of all-atom molecular dynamics simulations [26, 27] were extended here to a total of 80 ns. A table describing the conditions and the duration of all the simulations considered in this study is included in Online resource 1, Table 1.

Sufficient sampling of the configurational portion of phase space is a matter of considerable concern in macromolecular dynamics simulations [26, 42, 43]. Those studies and others [44–46] indicate that more effective sampling of the conformational space of proteins is obtained from multiple short trajectories starting from a single conformation with the use of different random distributions for the initial velocities rather than from a single, long trajectory.

In general, it has been observed that a single longer trajectory samples only one region of configurational space [43, 47], whereas multiple shorter trajectories starting from the same configuration with different initial velocities sample multiple nearby regions of configurational space [43, 45, 47, 48]. That is, multiple shorter simulations allow for the sampling of different regions of phase space, and so a set of these trajectories is necessary to have reasonable phase-space coverage. Hence, structural and dynamic properties obtained from multiple trajectories are improvements of those obtained from single longer trajectories [43, 45, 48]. In this work, fluctuations about the native-state and perturbations due to carboplatin and cisplatin binding were sampled by multiple molecular dynamics simulations with different initial atomic velocities.

Representative ensemble of structures

The last 12 ns of each of the four independent simulations were considered for analysis. Snapshots, each containing a record of all atom positions in the protein-DNA complex at a given time, taken every 20 ps intervals from the trajectories of the simulated MutSα-carboplatin-damaged-DNA complex, were collected to obtain a representative ensemble of structures. Only the protein complex was included in the snapshots. Similar representative ensembles of structures were generated for the cisplatin-damaged and mismatched DNA MutSα recognition complexes.

Nonbonding interactions energy calculations

Protein-protein and protein-DNA electrostatic and van der Waals nonbonding interactions energies were calculated from the trajectories by applying CHARMM [29] interaction energy analysis to the collected snapshots. Coulomb's electrostatic interactions and van der Walls interactions based on 6 and 12 Lennard-Jones

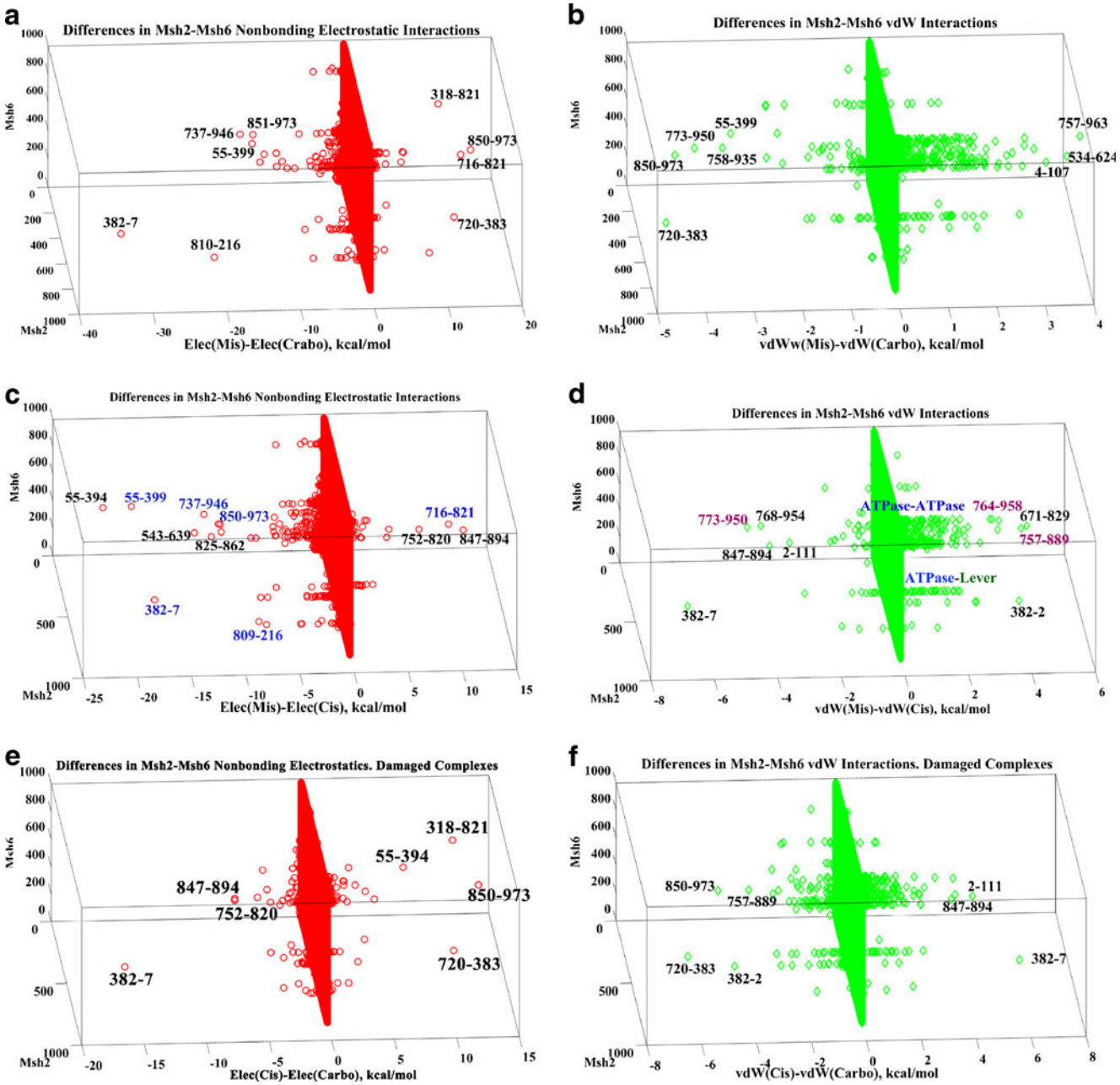

Fig. 3 Energy differences at the MutSα's interface from representative structures of the mismatched and damaged DNA recognition complexes differences in the electrostatic (**a**) and van der Waals (**b**) interactions at the protein-protein interface between carboplatin-damaged and mismatched recognition complexes. **c** In blue are common or similar differences in the nonbonding electrostatic interactions at the protein interface between the cisplatin-damaged and mismatched DNA recognition complexes. **d** In magenta are common or similar differences in the van der Waals interactions at the protein interface between the cisplatin-damaged and mismatched DNA recognition complexes. As in carboplatin-damaged DNA recognition complex, most differences in no-specific interactions at the protein interface derive from interactions of lever and ATPase domains of Msh2 with ATPase domain of Msh6. **e** Indicates particularly strong electrostatic interactions specific to the carboplatin-damaged complex, namely 850–973, 318–821,720–383, and 55–394, as well as particularly strong electrostatic interactions specific to the cisplatin-damaged complex, namely 382–7 and 847–894. **f** Indicates strong van der Waals interactions specific to cisplatin-damaged complex, 720–383, 850–973, 383–2 and 757–889, as well as strong van der Waals interactions specific carboplatin-damaged complex, namely 382–7, 2–111 and 847–894. Residue pairs herein are in Msh2-Msh6 format

potential were shifted to zero using a cutoff value of 22 Å. Any interactions beyond 22 Å were discarded. The spherical cutoff shifting criterion was applied on an atom by atom basis, method which has been proved [49] to be able to approximate no-cutoff results (computationally unfeasible for this large system) when a cutoff at or beyond 12 Å is used. A cutoff radius of 24 Å was used to generate the non-bonded pair list, and the non-bonding list was updated at every step. The solvent serves the dual

Table 1 Protein-protein interactions in carboplatin-damaged and mismatched MutSα recognition complexes, mean(std), kcal mol^{-1}

	Carboplatin	Mismatched
Msh2-Msh6 elect.	−140.68(30.97)	−2282.50(91.61)
Msh2-Msh6 vdw	−377.59(18.49)	−189.85(10.26)
Msh2 self elect.	−2017.51(39.74)	−24440.00(147.61)
Msh6 self elect	−2802.50(46.06)	−29272.00(224.38)
Msh2 self vdw	−3422.21(46.63)	−1147.50(26.31)
Msh6 self vdw	−3839.60(67.25)	−1343.80(31.30)

function of solvating each individual charge of the simulated protein-DNA complex and of screening the interaction between charge pairs. To approximate the solvent screening without including explicit water molecules, electrostatic interactions were calculated using a distance-dependent dielectric coefficient (RDIE [49] implemented in CHARMM [29]), **(r)=4r.**

Solvent accessible surface area calculations

The topology of the surface of a protein is intimately related to its function. Solvent accessible surface area (SASA) calculations for the damaged and mismatched MutSα-DNA recognition complexes were performed using the analytical method to compute the Lee and Richards surface [50], as implemented in CHARMM [29]'s *Coordinate Manipulation Commands* module. In the Lee-Richards surface the molecular system is represented by a set of interlocking spheres of appropriate van der Waals' radii and the accessible surface is traced out by the center of a spherical probe representing the solvent, as it rolls over the molecular systems' surface. CHARMM27 [32] force field's van der Waals radii for the nucleic acids, CHARMM22 [33] force field's van der Waals radii for the protein, and a spherical probe of 1.4 Å for water were used to calculate SASA based on the analytical method. Solvent accessible surface area per residue was calculated as mean value over the trajectories in each system.

For each of the representative ensemble of structures, the contact surface between the two subunits was calculated as the following: for example, for a given structure, the contact surface for Msh2 was calculated as the difference between the SASA of Msh2 alone and the SASA of Msh2 when Msh6 was present. Similarly, the contact surface for Msh6 was calculated as the difference between the SASA of Msh6 alone and the SASA of Msh6 when Msh2 was present.

SASA relation to hydrophobic effect: each square Angstrom of accessible surface area removed from contact with water gives a free energy gain of 25 kcal mol^{-1} [51, 52].

Contact maps

The center-of-geometry distance matrixes between residues, weighted average of residues, were computed from the trajectories using the *Coordinate Manipulation Commands* module in CHARMM [29] for several contact cutoff distances (20, 10, and 5 Å, respectively).

Hydrogen bonding analysis

Hydrogen bonding analysis was performed using the hydrogen bond analysis tool *hbond* from CHARMM [29], based on purely geometrical criteria of search for hydrogen bonding. As a special case of dipole interactions, hydrogen bonding or rather "hydrogen bridging" is defined as the attractive force between the hydrogen covalently bound to an electronegative atom of one molecule and an electronegative atom of another molecule or chemical entity. Usually, the electronegative atom is oxygen, nitrogen or fluorine, but hydrogen attached to carbon can also participate in hydrogen bonding when the carbon atom is bound to electronegative atoms [53]. In the strong/weak convention to characterize hydrogen bonding in biomolecules [54–56], its definition of strong or weak takes into account the electronegativity of the hydrogen's donor and acceptor. Following the above convention, in this study strong hydrogen bonding or hydrogen bonding refers to strong donor-strong acceptor interactions, such as in O–H…O, N–H…O, O–H…N, and N–H…N. The criterion for hydrogen bonding interactions in this study was defined as having a separation distance $d \leq 3.0$ Å between the hydrogen atom and acceptor atom, and the cutoff for the angle θ between the donor-H…acceptor was set at 90^0, $90^0 < \theta \leq 180^0$. Hydrogen bonds mediated or formed by water molecules with the protein are beyond the scope of this analysis and were not considered.

Salt bridging analysis

Salt bridges were evaluated according to the distance between the charged donor atoms, positively charged Nζ of lysine, or Nζ, Nη1 and Nη2 of arginine, and the charged acceptor atoms, negatively charged Oε1 and Oε2 of glutamic acid, or Oδ1 and Oδ2 of aspartic acid, in the protein, and oxygen atoms in the phosphate group of the DNA nucleotides. The backbone of polynucleotides are highly charged, double stranded DNA having two negative charges per base-pair, one unit negative charge per phosphate group. A distance ≤4 Å, found as a "working definition" for an ion-pair based upon analysis of charged groups in 38 proteins [57], was employed. Applied to the collected snapshots from the trajectories, the salt bridge calculations were performed in CHARMM.

Clustering analysis

To determine the occupancy of different conformations during the time course of the simulations clustering analysis was performed. The clustering was performed based on the root

mean-square distances between conformations comprising the trajectories, calculated across all residues. The conformations were grouped together using distances in the coordinates space, as a measure of conformational similarity, using the ART-2′ algorithm [58] as implemented in CHARMM. The conformation closest to the cluster's center was considered as being representative of the class of structures making up the cluster, and these conformations were further analyzed. The conformations generated in this fashion, 14 for the carboplatin-damaged, 12 for the cisplatin-damaged, and eight for the mismatched MutSα-DNA recognition complex, were weighted in the overall trajectories (data presented in Online resource 2, Fig. 1) and were further investigated for similarities.

Their hierarchical clustering dendrogram, constructed using the agglomerative method of average linkage implemented in Matlab [58], presented in Online resource 2, indicate that the representative conformations for the carboplatin-damaged MutSα-DNA recognition complex are substantially different than the representative conformations for the mismatched MutSα-DNA recognition complex. The affinity for clusters is the relative RMSD between the conformations and at each particular stage the method joins together the two clusters that are the most similar, or have the highest affinity.

Histograms were generated with Matlab [59]; *t*-test analysis was performed using Matlab; structural details were rendered with VMD [31].

Results and discussion

Functional proteins are dynamic structures that allow for certain types of internal motion to enable their biological function. In the emerging view of allosteric regulation in proteins function, in which an event in one place at a protein structure causes an effect at another site, ligand interactions at the binding site causes changes in the protein conformational distribution that lead to altered protein activity. In our investigated system, the "default" function of MutSα is to recognize and to initiate repair of post-replicative DNA errors through the MMR-repair pathways. The "altered" activity of MutSα can be considered the recognition of damaging, platinum-based DNA adducts and consequently the initiation of cell death by MMR-dependent apoptosis pathway.

We have previously shown [27] that MutSα binding to the cisplatin-induced damaged DNA adduct alters the protein dynamics around the native state, providing evidence on the molecular origin of the MMR-apoptotic pathway. Here, through means of nonbonding interactions energies, solvent accessible surface area, hydrogen bonding and salt bridges we investigate and quantify conformational and structural changes at the MutSα's protein-protein interface in response to the binding to the 1,3-d(GXG) intra-strand platinum-DNA adduct (the main adduct induced by chemotherapeutical agent carboplatin) by comparison with protein-protein interactions in the mismatched DNA recognition complex.

Nonbonding interactions at the protein-protein interface and MutSα' subunits self-interactions

Msh2-Msh6 nonbonding interactions energies over the course of our simulations were used as an indication of the degree of dimerization between the protein's monomers in response to carboplatin-damaged and mismatched DNA substrates recognition. These data suggest a severe impairment of the dimerization of MutSα and structural rearrangements at the protein-protein interface and within subunits in response to damaged DNA recognition.

The electrostatic (specific) and van der Waals (non-specific, induced dipole) interactions were calculated in an implicit solvent approximation using a distance-dependent dielectric to mimic the screening effect of the solvent (see "Methods"). The histograms of the nonbonding interactions at the protein-protein interface and the MutSα's subunits self-interaction energies in the carboplatin-damaged and mismatched recognition complexes are presented in Fig. 2a–f. Their average values from the simulations are presented in Table 1. Similar results are seen in the cisplatin-induced damaged DNA MutSα recognition complex, Online resource 2.

MutSα dimerization seems to be severely impaired in response to damaged DNA recognition

Data in Table 1 indicate that, while in the mismatch recognition complex electrostatic interactions are dominant at the protein-protein interface and within subunits, in the damage recognition complex the disperse forces interactions are dominant. Overall, the nonbonding interactions are about five times weaker at the MutSα's protein-protein interface in the damage recognition complex than in the mismatch recognition complex. In addition, while self-electrostatic interactions within subunits are indicated about 10 times weaker in response to damaged DNA recognition, the van der Waals interactions within subunits are about three times stronger in response to damaged DNA recognition than in response to the "default" mismatched DNA recognition.

These major differences in interactions energies suggest the possibility of significant conformational and structural changes at the protein-protein interface and within subunits in response to damaged DNA recognition.

Specific interactions at the MutSα's protein-protein interface in damaged versus mismatched DNA recognition complexes

To investigate the specific interactions responsible for the large differences on nonbonding interactions energies at the MutSα's protein-protein interface in the damaged and mismatched DNA

recognition complexes, the Msh2-Msh6 interactions per residue were calculated for the representative structures indicated by clustering analysis (the structures representing the center of the most populous cluster in each system and proved to be substantially different, see the clustering analysis in the Methods section and the dendrogram of the representative structures included in the Online resource 2, Fig. 1), and their differences are presented in Fig. 3.

These data indicate not only strong differences in the nonbonding interactions at MutSα's interface in the damaged versus mismatched DNA recognition complexes (Fig. 3a–d), but also significant differences between the carboplatin and cisplatin damaged DNA recognition complexes (Fig. 3e and f). The main differences in the electrostatic interactions (Fig. 3a, c, and e) derive from interactions of the mismatch binding, lever and ATPase domains of Msh2 with lever, mismatch binding and ATPase domains of Msh6, respectively. The main differences in the van der Waals interactions (Fig. 3b, d, and f) derive from interactions of the mismatch binding domain of Msh2 with the mismatch binding and lever domains of Msh6, lever domain of Msh2 with the mismatch domain of Msh6, clamp domain of Msh2 with the clamp domain of Msh6, and the ATPase domain of Msh2 with the lever and ATPase domains of Msh6.

Differences in the electrostatic interactions

Overall, data indicate that carboplatin-damaged DNA recognition induces stronger differences in the electrostatic interactions at the protein-protein interface than the cisplatin-damaged DNA recognition, when compared with the mismatched DNA recognition. Specifically, about 15 kcal mol^{-1} stronger interactions, as indicated in Fig. 3a and c and confirmed in Fig. 3e.

Most of the protein-protein electrostatic interactions responsible for the main differences between mismatched and damaged DNA recognition complexes are common or similar for both carboplatin and cisplatin damages, namely the interactions between residue pairs 55–399, 382–7, 716–821, 737–946, 809–216 or 810–216, 850–973 (data labeled in blue in Fig. 3c).

However, some of these particularly strong common electrostatic interactions at the protein-protein interface are indicated as specific to the carboplatin-induced damage, specifically the interactions between residue pairs 850–973, 318–821, 720–383, and 55–394, while others are indicated as specific to the cisplatin-induced damage, such as the electrostatic interactions between residue pair 382–7 (Fig. 3e). Particularly strong and specific to the later damaged DNA recognition complex are also indicated the 382–7 and 847–894 electrostatic interactions, Fig. 3e; the 382–7 electrostatic interaction is indicated as weaker than in the mismatched complex but stronger than in the carboplatin complex and the 847–894 interaction is indicated as stronger than in both mismatched and carboplatin recognition complexes. All interactive residue pairs are described in the Msh2-Msh6 representation.

Differences in the van der Waals interactions

On the contrary, overall, data indicate that the cisplatin-damaged DNA recognition induces slightly stronger differences in the van der Waals interactions at the protein interface than the carboplatin-damaged DNA recognition, when compared with the mismatched DNA recognition. Specifically, about 7 kcal mol^{-1} stronger interactions, as indicated by data in Fig. 3b and d and confirmed by data in Fig. 3f.

As pointed out above, the most significant differences in the van der Waals interactions at the MutSα's interface in damaged versus mismatched, as well as between the two damaged DNA recognition complexes, are predicted as interactions between the ATPase domain of Msh2 and the lever and ATPase domains of Msh6 (the labeled regions in Fig. 3d). Some of the strongest, nonspecific interactions at the protein-protein interface are common or similar for both carboplatin and cisplatin damaged DNA recognition complexes, and they are indicated in magenta in Fig. 3d. Specifically, these are the interactions between the residue pairs 764–958 or 758–935, 757–889 or 757–963, and 773–950.

However, these calculations also indicate several significant differences in the nonspecific interactions at the protein interface in the two damaged DNA recognition complexes. To this end, data in Fig. 3f suggest that the 720–383, 850–973 382–2 and 757–889 interactions seem to be specific to the cisplatin-damaged complex, while the 382–7, 2–111 and 847–894 interactions seem to be specific to the carboplatin-damaged complex. All interactive residue pairs are described in Msh2-Msh6 representation.

Structural changes derived from differences in interactions at the MutSα interface: mismatched versus damaged

Highlighted in Fig. 4 are regions at the MutSα's protein-protein interface predicted to be responsible for energy differences higher/lower than ±5 kcal mol^{-1} in electrostatic interactions and ±2 kcal mol^{-1} in van der Waals interactions.

In regard to the regions responsible for the significant differences in the electrostatic interactions (Fig. 4a): depicted in magenta for Msh2's residues and in blue for Msh6's residues, the strong, specific interactions corresponding to the mismatched versus damaged differences lower than −5 kcal mol^{-1} are located at the (1) clamp-clamp, (2) mismatch binding-mismatch binding, (3) lever-mismatch binding, (4) mismatch binding-lever, (5) ATPase-connector, (6) ATPase-lever, and (7) ATPase-ATPase interfaces. On the contrary, several strong, specific interactions (depicted in lime for Msh2's residues and in yellow for Msh6's residues) at the (5) ATPAase-connector, (8) lever-ATPase, and (7) ATPase-ATPase interfaces in the

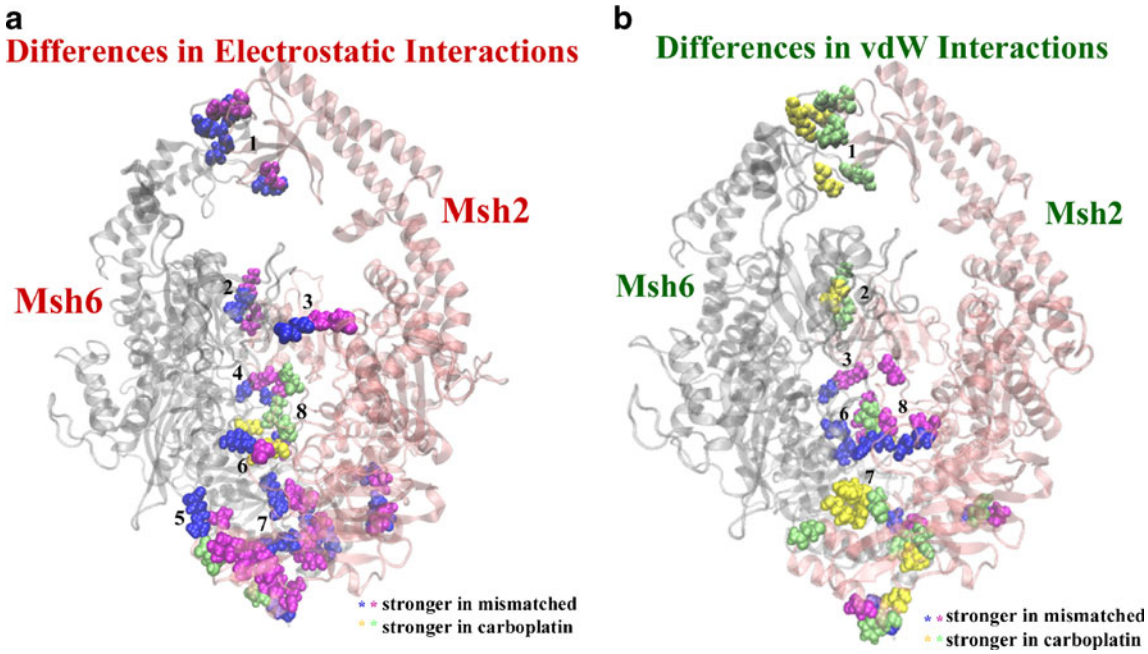

Fig. 4 Mapping structural changes as derived from the differences in nonbonding interactions at the MutSα's interface differences higher/lower than ±5 kcal mol^{-1} in electrostatic interactions and±2kcal mol^{-1} in van der Waals interactions were considered. **a** Differences in electrostatic interactions: strong, specific interactions (depicted in magenta for Msh2's residues and in blue for Msh6's residues) at the (1) clamp-clamp, (2) mismatch binding-mismatch binding, (3) lever-mismatch binding, (4) mismatch binding-lever, (5) ATPase-connector, (6) ATPase-lever, and (7) ATPase-ATPase Msh2-Msh6 interfaces in the mismatched DNA recognition complex weaken in the carboplatin-damaged DNA recognition complex; strong, specific interactions (depicted in lime for Msh2's residues and in yellow for Msh6's residues) at the (5) ATPAase-connector, (8) lever-ATPase, (7) ATPase-ATPase Msh2-Msh6 interfaces in the carboplatin-damaged DNA recognition complex weaken in the mismatched DNA recognition complex. **b** Differences in van der Waals interactions: are dominated by stronger interactions at the (1) clamp-clamp, (2) mismatch binding-mismatch binding, and (7) ATPase-ATPase Msh2-Msh6 interfaces (interactions depicted in lime-yellow) in the carboplatin-damaged DNA recognition complex; several sites with stronger van der Waals interactions at the (6) ATPase-lever and (8) lever-ATPase Msh2-Msh6 interfaces in the mismatched DNA recognition complex are also predicted (interactions depicted in magenta-blue). Overall, strong, specific electrostatic interactions at the protein-protein interface in the mismatched recognition complex are replaced by weak, non-specific van der Waals interactions in the carboplatin-damaged recognition complex

carboplatin-damaged DNA recognition complex weaken in the mismatched DNA recognition complex (mismatched versus damaged differences higher than 5 kcal mol^{-1}).

In regard to the regions responsible for the significant differences in the van der Waals interactions (Fig. 4b): depicted in lime for Msh2's residues and yellow for Msh6's residues, the interactions corresponding to the mismatched versus damaged differences higher than 2 kcal mol^{-1} are located at the (1) clamp-clamp, (2) mismatch binding-mismatch binding, and (7) ATPase-ATPase interfaces. Additionally, several sites with stronger van der Waals interactions at the (6) ATPase-lever and (8) lever-ATPase interfaces of the mismatched DNA recognition complex than of the damaged DNA recognition complex are also predicted (interactions depicted in magenta-blue; mismatched versus damaged differences lower than −2 kcal mol^{-1}).

Overall, strong, specific electrostatic interactions at the protein-protein interface of MutSα in the "default" mismatched DNA recognition complex are replaced by weaker non-specific van der Waals interactions in the "altered" carboplatin-damaged DNA recognition complex.

Structural details derived from differences in interactions at the protein-protein interface of MutSα in the carboplatin versus cisplatin damaged DNA recognition complexes, along with a comprehensive conformational analysis of the two systems will be the subject of a future investigation in our group.

It can be concluded that nonbonding interactions at the MutSα heterodimer interface suggest a severe impairment of the protein dimerization in response to damaged DNA recognition. In the following section, by means of solvent accessible surface area calculations we will try "to quantify" the alteration of the MutSα's dimerization and to address the question of whether either hydrophobic forces or stronger van der Waals interactions are possibly responsible for structural rearrangements in response to damaged DNA recognition.

Solvent accessible surface area calculations

Indicating significant structural changes in response to damaged DNA recognition, the mean values for the solvent accessible surface area (SASA; see "Methods") of the Msh2 and Msh6 subunits, along with SASA of their charged residues are

presented in Table 2. Histograms of SASA that are indicated in Table 2 to undergo statistically significant changes in response to damaged DNA recognition are included in Fig. 5a and b. These data also suggest that, by comparison with the mismatched DNA recognition, the MutSα binding to the carboplatin-damaged DNA allosterically regulates the protein's dynamics at the Msh2-Msh6 interface in a different manner, and, subsequently, may induce a different than repair functional response of the protein.

van der Waals interactions possible responsible for different packing in response to damaged DNA recognition by MutSα

Specifically, in the damage recognition complex, the mean SASA of the Msh2 subunit is indicated to be about 714 Å^2 higher than in the mismatch recognition complex. These data are presented in Table 2 and their statistical analysis is included in Online resource 2, Table 2 . How precisely to extra the degrees of freedom from this data, and the data below in Table 3, is not entirely clear. At one extreme, in Online resource 2, Tables 2 and 3, each structure from the equilibrated ensemble of structures (last 12 ns of each of the independent simulations, see "Methods") could be considered as an individual uncorrelated data point. At this extreme, all of the results are statistically significant with p-values$\leq$0.001. The other extreme is to consider each independent simulation as a data point. The later extreme is clearly too pessimistic as that would the results from an ideal—i.e., infinitely long—simulation insignificant. However, the extreme of considering each structure independently is likely too optimistic. Given that for our simulated systems, most of the equilibration occurs within the first 2 ns (see "Methods") and the last 12 ns of the 20 ns long simulations were considered for analysis, it would be reasonable to consider the relaxation time as on the order of nanoseconds and so the number of independent samples is in the 10s. As a result, as shown in Online resource 2, Tables 2 and 3, the largest two changes in Table 2 are statistically significant. A commonly-accepted relation of SASA to hydrophobic effect: each square Angstrom of accessible surface removed from contact with water gives a free energy gain of 25 kcal mol^{-1} [51, 52]. Consequently, no significant change in Msh6's SASA and higher Msh2's SASA in response to damaged DNA recognition would suggest that hydrophobic forces may not be responsible for the impairment of the MutSα's dimerization in response to damaged DNA recognition.

Table 2 Solvent accessible surface area calculations, mean(std) Å^2, in the mismatched and carboplatin-damaged DNA MutSα recognition complexes

	Mismatched	Carboplatin
Msh2	36926.58(579.57)	37640.63(512.66)
Msh6	42238.64(635.67)	42278.95(989.03)
ch_Msh2	16316.11(400.14)	16644.35(362.10)
ch_Msh6	19438.87(375.65)	19451.35(395.97)

"ch" indicates charged residues

However, higher solvent accessible surface area of the charged residues in the Msh2 subunit (Table 2) would indicate a rather different "pose" of the signaling subunit in response to damaged DNA recognition.

Corroborated with the above observations derived from calculations of the nonbonding interactions, the SASA calculations suggest the possibility of a different packing at the protein-protein interface and within subunits in response to damaged DNA recognition.

Advancing our investigation into the MutSα's structural changes in response to the damaged DNA recognition, surface representations of representative structures for both mismatched and carboplatin-damaged recognition complexes are included in Fig. 6. These representations reveal a more compact protein, especially the Msh6 subunit, in response to damaged DNA recognition by comparison with the "default" mismatched DNA recognition complex, in which multiple channels and larger cavities are indicated in both subunits.

Loss of contact at the MutSα's interface in response to damaged DNA recognition

To further analyze changes at the MutSα's interface in response to damaged DNA recognition, the area of the contact surface between the two subunits as well as the area of the charged residues in the contact surface as seen by a spherical probe of 1.4 Å, were calculated in both damage and mismatch recognition systems. Mean values and standard deviations for these data are included in Table 3, and their statistical analysis is included in Online resource 2, Table 3, and the statistical analysis is discussed above with Table 2. Histograms of these calculated quantities are included in Fig. 5c–e.

These data (Table 3) indicate a significant decrease of the mean values of the contact surface area for both Msh2 and Msh6 subunits, by about 252 Å^2 and 375 Å^2, respectively, in the damaged DNA recognition complex, "quantifying" the loss of the degree of dimerization of the heterodimer indicated by the nonbonding interactions at the protein-protein interface.

Additionally, these data (Table 3) hint a significant decrease of the mean value of the area of the Msh6's charged residue in the protein-protein contact surface in response to damaged DNA recognition, by about 140 Å^2. This finding corroborates with the decrease of electrostatic interactions at the MutSα's protein-protein interface, as indicated by nonbonding interactions, and supports the general observation of structural rearrangements in response to damaged DNA recognition.

Structural details of the changes at the MutSα's protein-protein interface, defined here as atoms of each of the two monomers as well as of the solvent within 5 Å, are presented

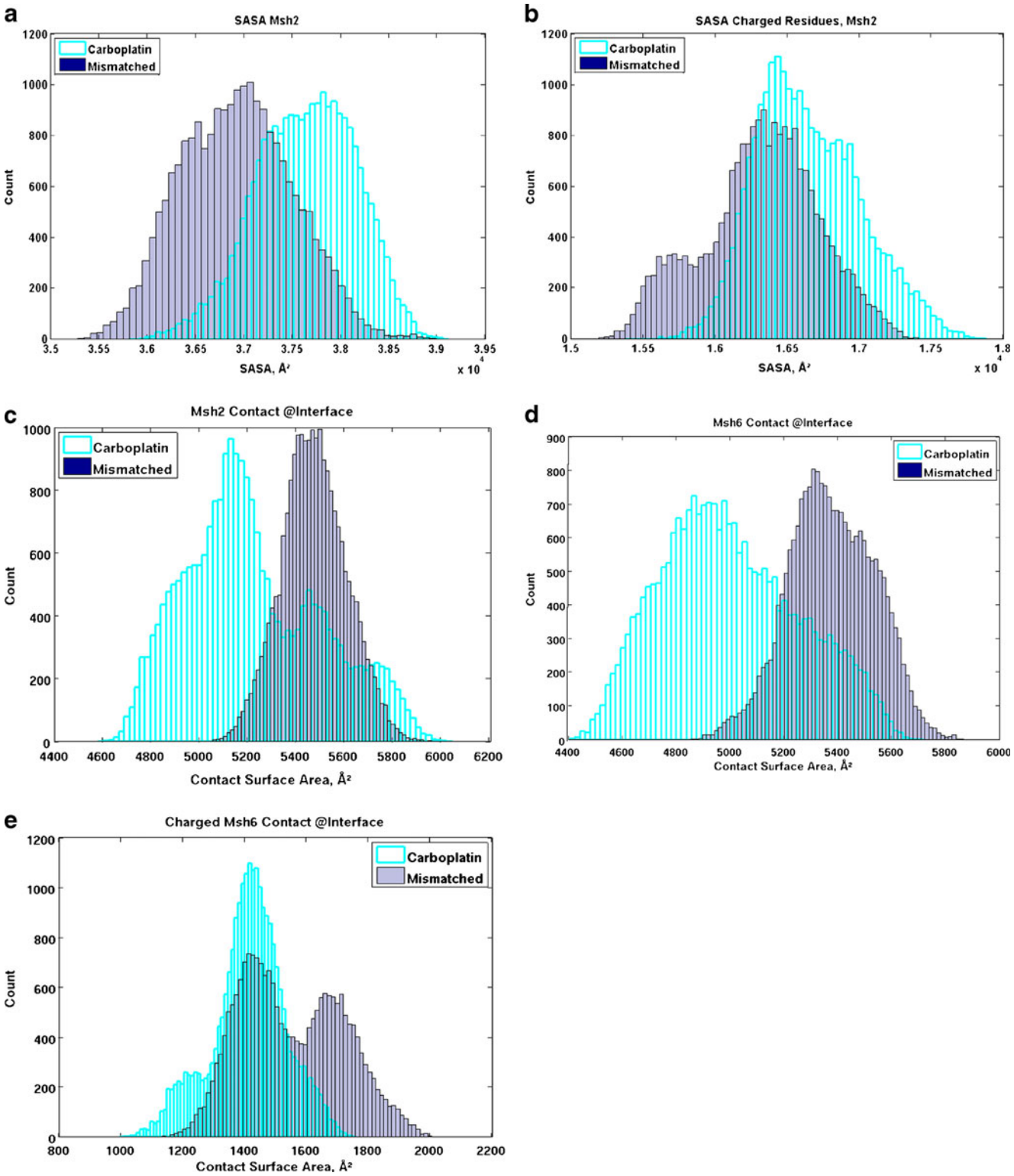

Fig. 5 Solvent accessible surface area (SASA) analysis. **a** The mean of SASA of Msh2 subunit in the carboplatin-damaged complex, 37640.63(512.66) Å^2, is higher than in the mismatched complex, 36926.58(579.57) Å^2. **b** The mean of SASA of the charged residues of Msh2 in the carboplatin complex, 16644.35(362.10) Å^2, is higher than in the mismatched complex, 16316.11(400.14) Å^2. **c** The mean of contact surface area of Msh2 at the protein-protein interface in the carboplatin complex, 5222.39(280.33) Å^2, is lower than in the mismatched complex, 5474.91(134.88) Å^2. **d** The mean of contact surface area of Msh6 at the protein-protein interface in carboplatin complex, 5000.48(255.37) Å^2, is lower than in the mismatched complex, 5376.15(159.18) Å^2. **e** The mean of contact surface area of the charged residues in Msh6 at the protein-protein interface in carboplatin complex, 1414.09(120.46) Å^2, is lower than in the mismatched complex, 1553.89(166.33) Å^2. The two populations corresponding to the mismatched recognition complex are simulation dependent, but not entirely (Online resource 3, a). Data presented are mean(std)

Table 3 Contact surface area between Msh2 and Msh6 subunits at the MutSα interface (Int.), mean(std) Å^2, in the mismatched and carboplatin-damaged DNA recognition complexes

	Mismatched	Carboplatin
Msh2@Int.	5474.91(134.88)	5222.39(280.33)
Msh6@Int.	5376.15(159.18)	5000.48(255.37)
ch_Msh2@Int.	1382.07(108.21)	1397.44(235.78)
ch_Msh6@Int.	1553.89(166.33)	1414.09(120.46)

in Fig. 7. Rendered from solvated representative structures indicated by clustering analysis, the structural details include a general view of the protein-protein interface, Fig. 7a and b, as well as "the pose" at the interface for each subunit in both carboplatin-damaged (Fig. 7c and d) and mismatched (Fig. 7e and f) DNA recognition complexes.

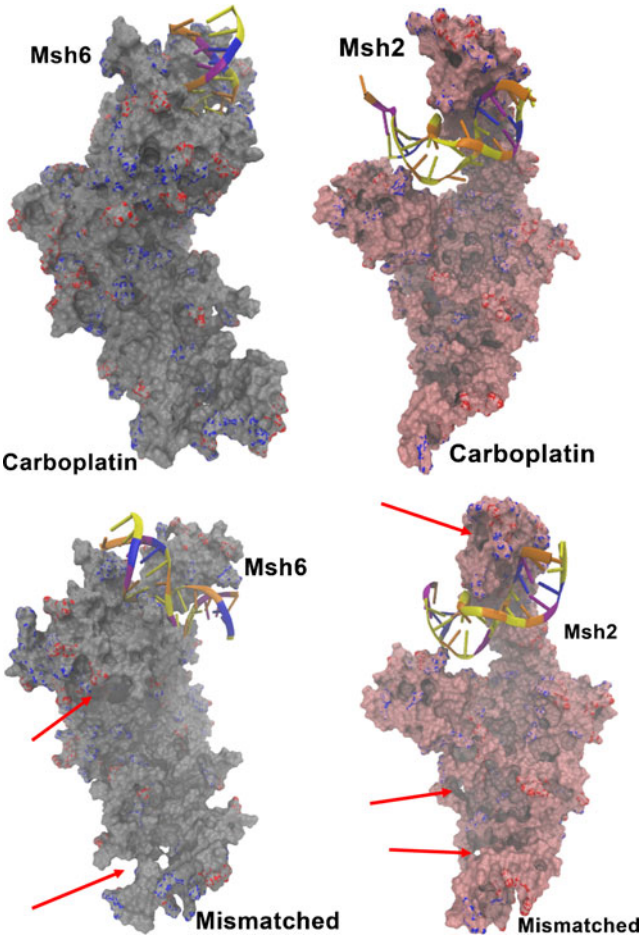

Fig. 6 Surface representation the carboplatin-damaged and mismatched MutSα-DNA recognition complexes. A more compact protein, especially the Msh6 subunit, is indicated in response to carboplatin-damaged DNA recognition by comparison with "the default" mismatched DNA recognition complex, in which multiple channels and larger cavities are indicated in both subunits. Positively charged residues at the protein surface are depicted in blue, while negatively charged residues are depicted in red. The surface representations are for representative structures indicated by clustering analysis of the dynamics trajectories in each system

These structural pieces of evidence indicate that in both damaged and mismatched DNA recognition complexes the protein-protein interface comprises residues from all five domains of each subunit of the protein, with ATPase domains being dominant, Fig. 7c–f.

However, even though the protein-protein interface in the damaged DNA recognition complex is indicated to extend over a larger number of residues, 127 from Msh2 and 137 from Msh6, as compared with the mismatched DNA recognition complex, 108 residues from Msh2 and 124 residues from Msh6, a higher presence of water molecules at the protein-protein interface in the damaged DNA recognition complex is noteworthy. These structural pieces of evidence support the SASA calculations indicating (1) a loss of contact at the MutSα's interface and (2) the possibility for water-mediated interactions in response to damaged DNA recognition. The latter observation is supported by higher exposure of charged residues on the Msh2 surface (Table 2). Beyond the scope of this investigation, the water-mediated protein-protein interactions in these MutSα-DNA recognition complexes is under consideration for a follow up study.

Similar protein core in response to damaged DNA recognition by MutSα

To further identify structural elements responsible for the major differences in nonbonding interactions at the MutSα's protein-protein interface and within subunits in response to damaged DNA recognition, major differences on the calculated solvent accessible surface area per residue (Fig. 8a and b), as well as the protein's core residues (Fig. 8c and d) in the two recognition complexes will be investigated next.

The mismatched versus carboplatin-damaged differences on the average SASA per residue indicate structural changes primarily in the mismatched binding and connector domains of the Msh2 subunit (Fig. 8a), and in the ATPase domain of the Msh6 subunit (Fig. 8b).

Specifically, in the Msh2 subunit (Fig. 8a) hydrophobic residues F286 and L258, polar residues N109 and N285, and positively charged K627 are indicated as more exposed to the solvent in the mismatched complex than in the carboplatin-damaged complex. On the contrary, hydrophobic F136 and L719, and positively charged R227 and K246 are indicated as more exposed to the solvent in the carboplatin-damaged complex than in the mismatched complex.

Specifically, in the Msh6 subunit (Fig. 8b) hydrophobic residues I601, L629, or I921, polar residue Q761, and negatively charged residues E758 and E911 are indicated as more exposed to the solvent in the mismatched DNA recognition complex than the carboplatin-damaged DNA recognition complex. Oppositely, hydrophilic residues F572 and M823,

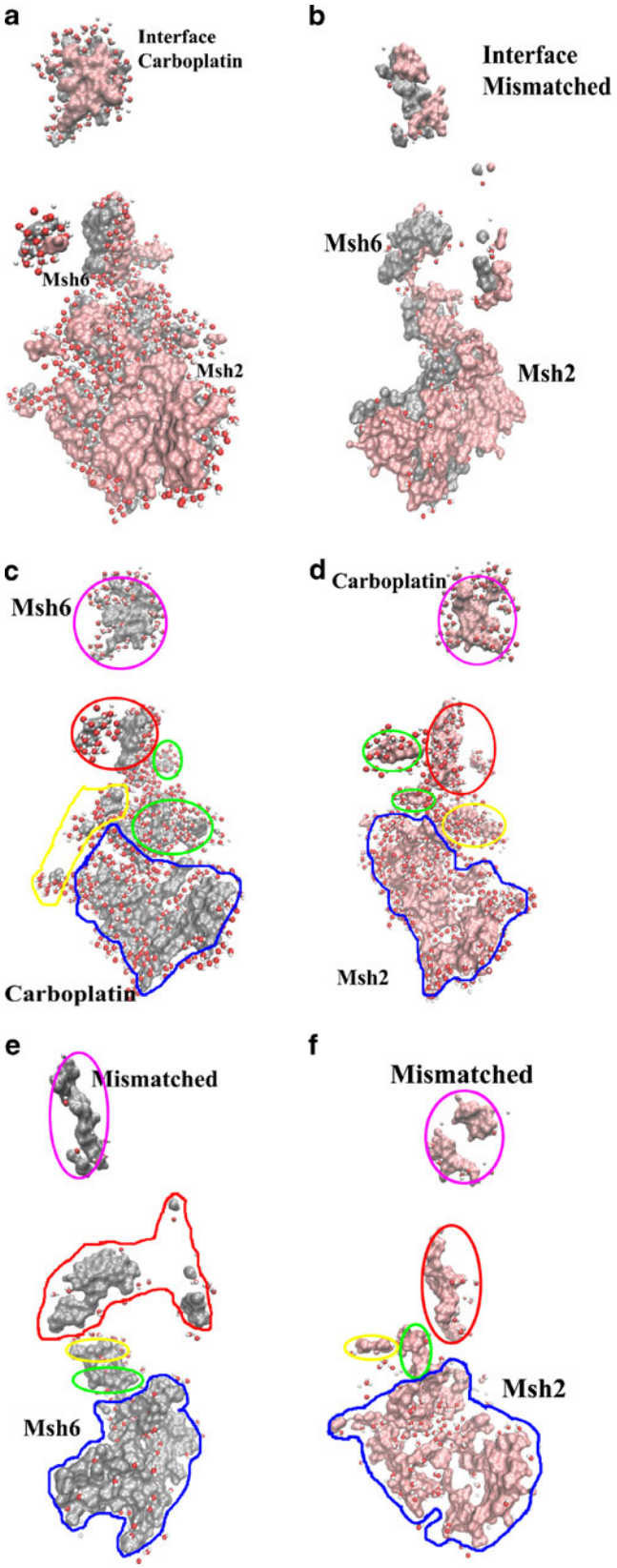

Fig. 7 Structural details at the MutSα's protein-protein interface in the damaged and the mismatched DNA recognition complexes protein-protein interface is defined here as atoms of each of the monomers as well as of the solvent within 5 Å. The Msh2 subunit is depicted in pink and the Msh6 subunit is depicted in silver. The water molecules are depicted in a ball-and-stick representation. The presented structural details are for solvated representative conformations identified by clustering analysis. They include a general view of the above defined interface, **a** and **b**, as well as "the pose" at the interface for each subunit in both carboplatin-damaged (**c** and **d**) mismatched (**e** and **f**) DNA recognition complexes. The protein-protein interface comprises atoms from all five domains of the heterodimer protein in both recognition complexes, as indicated my marked region: red for the mismatched binding domain; yellow for the connector domain; green for the lever domain and blue for the ATPase domain in **c**–**f**. By comparison, even though the protein-protein interface in the carboplatin-damaged DNA recognition complex (**c** and **d**) extends over a large number of residues, 127 from Msh2 and 137 from Msh6, versus 108 residues from Msh2 and 124 residues from Msh6 in the mismatched DNA recognition complex (**e** and **f**), a higher content of water molecules is indicated at the protein-protein interface in response to damaged DNA recognition

polar residues N763 and N912, and negatively charged residues E394 and D710 are indicated as more exposed to the solvent in the carboplatin-damaged DNA recognition complex than in the mismatched DNA recognition complex.

However, the core residues of MutSα—defined here as residues with solvent accessible surface area averaged over the simulations lower than 1 $Å^{2—}$ are indicated as conserved in response to damaged DNA recognition (Fig. 8c and d). These pieces of evidence support the general observation that the most significant structural changes in response to damaged DNA recognition may occur at the protein-protein interface and on the surface of the two subunits of the protein.

Rearrangement of contacts at the MutSα's interface in response to damaged DNA recognition

To further substantiate the general observation of structural rearrangements in response to damaged DNA recognition, changes in contacts between residues at the MutSα's protein-protein interface calculated from the average distance matrix were also investigated Fig. 8e and f.

For a cutoff distance of 20 Å, these data predict both a loss (Fig. 8e) of about 14% and a gain (Fig. 8f) of about 9% in the contacts between the residues at the protein-protein interface in response to damaged DNA recognition, suggesting an overall rearrangement of the contacts at the MutSα's protein-protein interface in response to damaged DNA recognition.

Specifically, apart from the contacts at the interface between the mismatched binding (residues 1–124) and connector (residues 125–297) domains of Msh2 and the ATPase domain (residues 715–974) of Msh6 (Fig. 8e), whose loss has no predicted corresponding gain (Fig. 8f), most of the lost or gained contacts are in similar regions at the MutSα's interface.

The gained contacts in response to the damaged DNA recognition are indicated mainly at the interfaces of the clamp (region marked in red in Fig. 8f) and ATPase domains (region

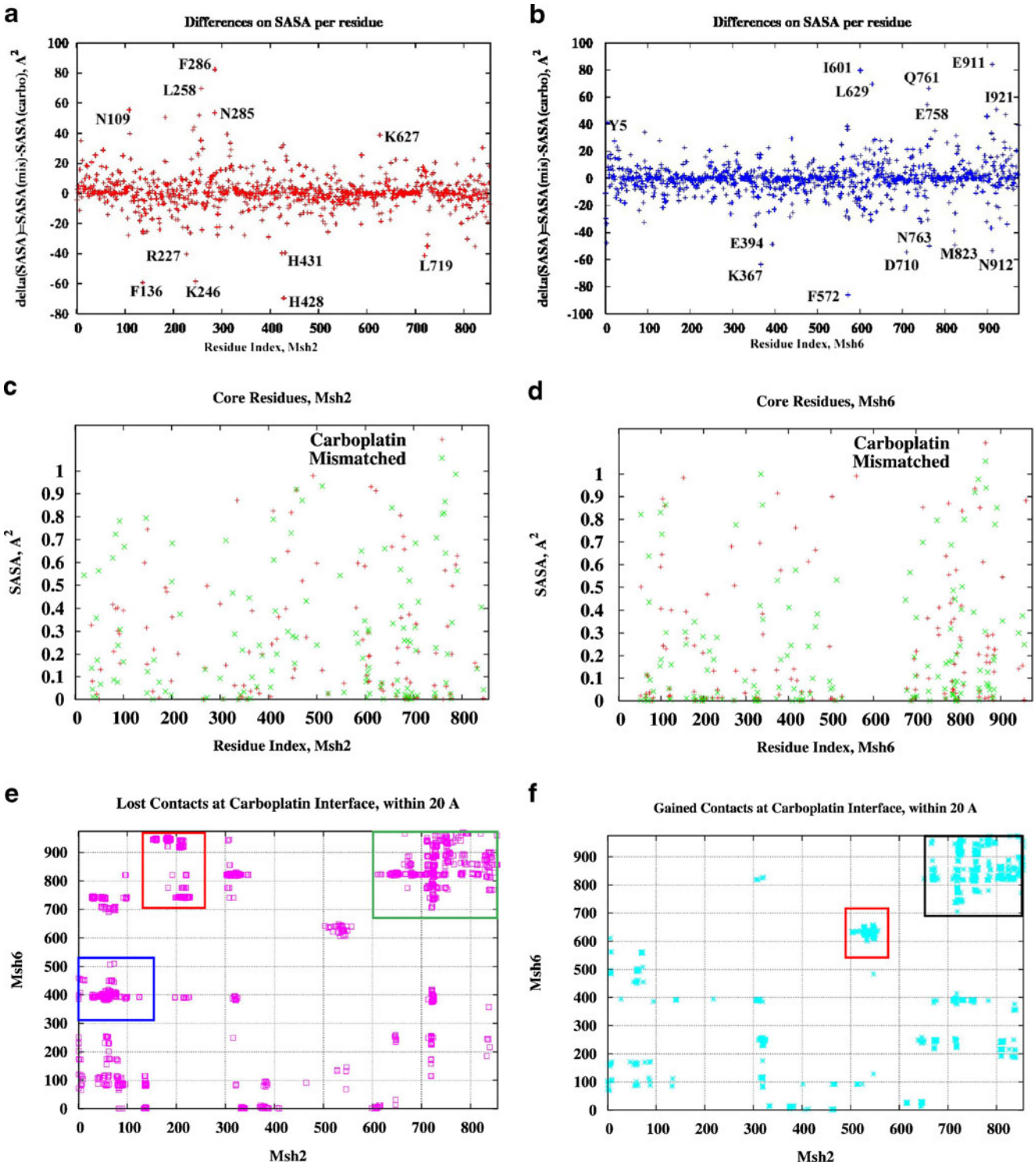

Fig. 8 Structural differences at the interface of the damaged DNA recognition complex revealed by SASA and contact maps calculations (**a** and **b**) The positive differences indicate residues more exposed to the solvent in the mismatched than in the carboplatin-damaged DNA recognition complex, while the negative differences indicate the opposite. **c** and **d** No significant changes are indicated on the core residues within both mismatched and carboplatin damaged recognition complexes. Core of the protein is defined here as composed of residues with solvent accessible surface area averaged over the simulations lower than 1 $Å^2$. **e** The lost contacts, about 1458, at the protein-protein interface in response to damaged DNA recognition are predominantly at the interface of the mismatched binding, the connector and the lever domains of Msh2 with the ATPase domain of Msh6. **f** The gained contacts, about 830, at the interface of the carboplatin–damaged DNA MutSα recognition complex are mainly at the ATPase-ATPase interface, suggesting, apart an overall rearrangement of the interactions at the protein-protein interface in response to damaged DNA recognition. The 2D contact maps were generated from the average distance matrix throughout the course of the trajectories in either system for a cutoff distance of 20 Å

marked in black in Fig. 8f) of the two subunits. These observations corroborate with the predicted stronger van der Waals interactions in these regions of the protein-protein interface, as discussed above and depicted in Fig. 4b.

On the other hand, the lost contacts at the protein-protein interface in response to damaged DNA recognition are indicated mainly at the interfaces of (i) the mismatched binding domain of Msh2 with the lever domain of Msh6 (region marked in blue in Fig. 8e), (ii) the connector domain of Msh2 with the ATPase domain of Msh6 (region marked in red in Fig. 8e), and (iii) the ATPase domains of the two subunits (region marked in green in Fig. 8e).

When contacts at the protein-protein interface within 10 Å are considered (Online resource 3, b), 53 or 8.4% of the contacts from the "default" mismatched DNA recognition complex are lost in response to the "altered" damaged DNA recognition. Furthermore, when contacts within 5 Å are considered (data not shown), MutSα's protein-protein interface losses five such contacts, namely 721–338 and 721–391 at the interface of the ATPase domain of Msh2 with the connector domain of Msh6, and 733–947, 836–837, and 844–869 at the interface of the ATPase domains of the two subunits. These observations further substantiate the overall conclusion of severe impairment of the MutSα's dimerization and structural rearrangements at the MutSα's protein-protein interface in response to damaged DNA recognition.

Point mutations studies of the residues predicted to differentiate the MutSα's protein-protein interface in the repair and cell-death conformations may allow the discovery of small ligands that would selectively induce these conformations, leading to new anticancer therapies targeting the MMR-dependent apoptotic pathway.

Correlated entities in the mismatched DNA recognition complex un-correlate or anti-correlate in response to damaged DNA recognition

Up to this point, structural interferences derived from non-bonding interactions, solvent accessible surface area, and contact map calculations suggest a severe impairment of the MutSα's dimerization by loss and rearrangement of interactions at the protein-protein interface.

In this concluding section of our study, possible correlations between hydrogen bonds, salt bridges, nonbonding interactions and solvent accessible surface area calculated from the trajectories are investigated. Correlation coefficients of the above entities are included in Online resource 4. 2D histograms of the representative cases are included in Figs. 9 and 10. Overall, these data point out that correlated entities in the mismatched DNA recognition complex un-correlate or anti-correlate in response to damaged DNA recognition, and their significance is summarized as following. The 2D histograms were generated using the *hist* and *contour* functions in Matlab. Normalizations were not performed so that the ranges of the data could be seen. The correlation coefficient for two given series of data collected for the representative ensemble of structures from trajectories, was calculated using the corrcoef function in Matlab. This function calculates the zeroth lag of the normalized covariance function, e.g., it calculates the t=0 value of the equal-time correlation function between two sets of data.

Fig. 9 Msh2 binding to the damaged DNA triggers non-specificity and destabilizing effects at the Msh2-Msh6 interface and within Msh6 subunit 2D histograms for the representative ensemble of structures are presented. **a** and **b** Uncorrelated ($r=0.07$) Msh2-DNA and Msh2-Msh6 strong hydrogen bonding in the mismatched DNA recognition complex are anti-correlated ($r=-0.40$) in the damaged DNA recognition complex. **c** and **d** Correlated ($r=0.56$) Msh2-DNA and Msh6-Msh6 strong hydrogen bonding in the mismatched DNA recognition complex are anti-correlated (r=−0.18) in the damaged DNA recognition complex. **e** and **f** Highly correlated ($r=0.63$) Msh2-DNA electrostatic interactions and Msh6 self-electrostatic interactions in the mismatched DNA recognition complex are weakly anti-correlated (r=−0.27) in the damaged DNA recognition complex. **g** and **h** Correlated ($r=0.45$) solvent exposed area of charged residues in Msh2 and Msh6 in the mismatched DNA recognition complex are anti-correlated ($r=-0.34$) in the damaged DNA recognition complex

Msh2 binding to the damaged DNA triggers non-specificity and destabilizing effects at the Msh2-Msh6 interface and within Msh6 subunit

While in the mismatched DNA recognition complex Msh2-DNA strong hydrogen bonding interactions seem to have no effect on the strong hydrogen bonding at the protein-protein interface (Fig. 9b, correlation coefficient $r=0.07$), on the contrary, in the carboplatin-damaged DNA recognition complex an increase in the number of Msh2-DNA strong hydrogen bonding interactions is accompanied by a decrease in the number of hydrogen bonding interactions at the protein-protein interface (Fig. 9a, $r=-0.40$). This finding can be seen as a destabilization of the heterodimer interface in response to damaged DNA recognition.

Additionally, Msh2 binding to the damaged DNA seems to trigger non-specificity and destabilizing effects within the mismatch recognition subunit, Msh6 (Fig. 9c–h).

Specifically, while in the mismatched DNA recognition complex an increase in the Msh2-DNA strong hydrogen bonding interactions is accompanied by an increase in the strong hydrogen bonding interactions within the mismatch recognition subunit Msh6 (Fig. 9d, $r=0.56$), on the contrary, in the damaged DNA recognition complex an increase in the Msh2-DNA strong hydrogen bonding triggers a decrease in the hydrogen bonding interactions within Msh6 subunit (Fig. 9c, $r=-0.18$). This finding can be seen as an internal destabilization of Msh6 by loss of specific interactions.

This propensity is also consistent with patterns observed in the nonbonding electrostatic interactions, as depicted in

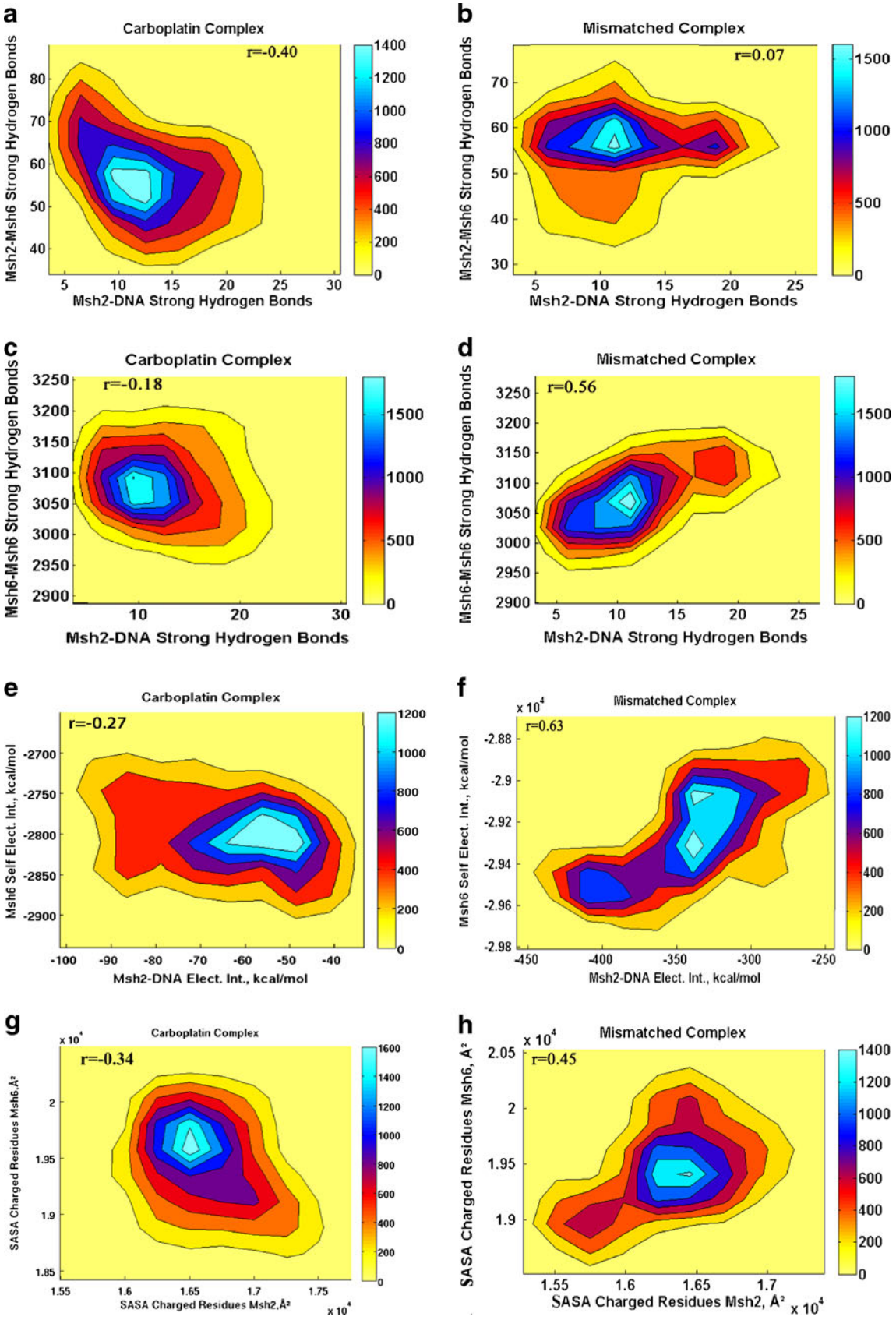
a
Carboplatin Complex
r=-0.40
Msh2-Msh6 Strong Hydrogen Bonds
Msh2-DNA Strong Hydrogen Bonds
b
Mismatched Complex
r=0.07
Msh2-Msh6 Strong Hydrogen Bonds
Msh2-DNA Strong Hydrogen Bonds
c
Carboplatin Complex
r=-0.18
Msh6-Msh6 Strong Hydrogen Bonds
Msh2-DNA Strong Hydrogen Bonds
d
Mismatched Complex
r=0.56
Msh6-Msh6 Strong Hydrogen Bonds
Msh2-DNA Strong Hydrogen Bonds
e
Carboplatin Complex
r=-0.27
Msh6 Self Elect. Int., kcal/mol
Msh2-DNA Elect. Int., kcal/mol
f
Mismatched Complex
r=0.63
Msh6 Self Elect. Int., kcal/mol
Msh2-DNA Elect. Int., kcal/mol
g
Carboplatin Complex
r=-0.34
SASA Charged Residues Msh6,Å²
SASA Charged Residues Msh2,Å²
h
Mismatched Complex
r=0.45
SASA Charged Residues Msh6, Å²
SASA Charged Residues Msh2, Å²

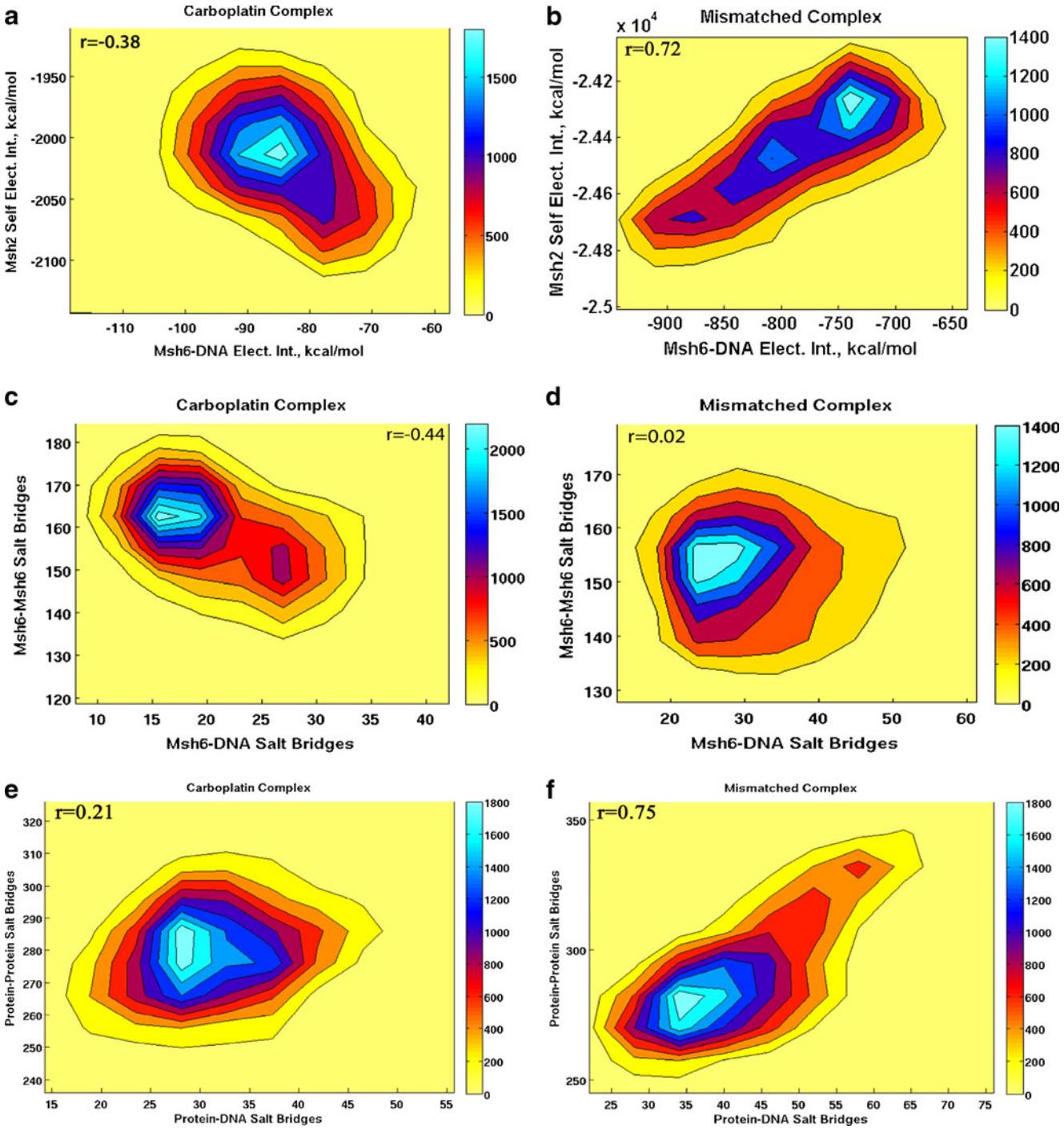

Fig. 10 Msh6 binding to the damaged DNA triggers non-specificity and destabilizing effects within both subunits. 2D histograms for the representative ensemble of structures are presented. **a** and **b** Synchronous Msh6-DNA electrostatic interactions and self-electrostatic interactions of the Msh2 subunit in the mismatched DNA recognition complex ($r=0.72$) become anti-correlated in response to damaged DNA recognition ($r=-0.38$). **c** and **d** Uncorrelated in response to mismatched DNA recognition ($r=0.02$), an increase in the number of specific ionic interactions at the Msh6-DNA interface triggers a decrease in the number of specific ionic interactions within the Msh6 subunit ($r=-0.44$). **e** and **f** Highly correlated in response to mismatched DNA recognition ($r=0.75$), protein-DNA and protein-protein specific ionic interactions (which includes salt bridges at the protein-protein interface and within subunits) are weakly correlated in response to damaged DNA recognition ($r=0.21$)

Fig. 9e and f. In this regard, while in the mismatched DNA recognition complex changes in the Msh2-DNA electrostatic interactions highly correlate with changes in the Msh6'self-electrostatic interactions (Fig. 9f, $r=0.63$), these entities are anti-correlated (Fig. 9e, $r=-0.27$) in response to the damaged DNA recognition.

Furthermore, synchronous changes in the solvent accessible surface area of the charged residues in Msh2 and Msh6 subunits

in the mismatched DNA recognition complex (Fig. 9h, $r=0.45$), becomes asynchronous in response to the damaged DNA recognition by MutSα (Fig. 9g, $r=-0.34$). This finding also supports the general observation of structural rearrangements in response to damaged DNA recognition: it indicates that an increase in the "presentation" of charged residues at Msh2's surface is accompanied by a decrease in the "presentation" of charged residues at Msh6's surface, or an increase in the buried charged residues in the Msh6 subunit.

It can be concluded that, unlike in the mismatched DNA recognition, Msh2 binding to the damaged DNA seems to send a distress signal through the mismatch recognition subunit and at the dimer's interface, which would possible trigger the MMR-dependent programmed cell death.

Msh6 Binding to the damaged DNA triggers non-specificity and destabilizing effects within both subunits

Interestingly enough, an analysis of the Msh6's interactions with the damaged DNA indicates similar effects, as presented in Fig. 10. To this end, synchronous Msh6-DNA electrostatic interactions and self-electrostatic interactions within the other subunit of the heterodimer, Msh2, in the mismatched DNA recognition complex ($r=0.72$, Fig. 10b), become anti-correlated in response to damaged DNA recognition ($r=-0.38$, Fig. 10a). This finding can be seen as a destabilizing effect on the Msh2 subunit in response to damaged DNA binding by the Msh6 subunit.

In the same context, uncorrelated in response to mismatched DNA recognition ($r=0.02$, Fig. 10d), an increase in the number of the specific ionic interactions at the Msh6-DNA interface triggers a decrease in the number of specific ionic interactions within Msh6 subunit in response to damaged DNA recognition ($r=-0.44$, Fig. 10c). This finding can be regarded as a destabilizing effect by loss of salt bridge interactions within Msh6 subunit upon its binding to the damaged DNA.

Finally, highly correlated in response to the mismatched DNA recognition ($r=0.75$, Fig. 10f), protein-DNA and protein-protein specific ionic interactions (which includes salt bridges at the heterodimer interface as well as within the subunits) become uncorrelated in response to damaged DNA recognition ($r=0.21$, Fig. 10e).

These data suggest that the loss of a synchronous mode of response while "surveying" post-replicative DNA would possibly be one of the cellular mechanism(s) of signaling the MMR-dependent programed cell-death much wanted in anti-cancer therapies.

Predictions from the current and similar simulations confirmed by experimental studies

Employing the same protocol, 2–10 ns of simulation of the *E. Coli* homologue molecular complex (MutS) have been experimentally verified to be sufficient to examine the experimental questions addressed [6, 7, 15]. Responses such as changes in disordered loops associated with the DNA damage response, conformational changes associated with ATP binding/hydrolysis, and key protein-DNA contacts predicted by conformational analysis of MutS complex with cisplatin-damaged DNA [5, 6] were validated by mutational and genetic analysis experiments [6].

Furthermore, the molecular dynamics simulations reported herein, predict conformational and structural DNA changes due to (1,3) cross-linking [60] that are in agreement with NMR structural studies on DNA structural changes due to (1,3) cross-linking, albeit without protein binding [22]. Specifically, in agreement with experimental observations [22], our simulations indicate that the distortion to DNA structure induced by carboplatin-based 1,3d(GpXGp) intra-strand platinum-DNA adduct spreads out over the entire lesion site, and it is most severe at the 5′ site. In this regard, the G8-C8 damaged base pair and the central C9-G7 base pair lost their hydrogen bonding during the entire simulations time. In agreement with experiment [22], our simulations also indicate that the central base C9 is extruded from the minor groove. At the 3′ end, less distorted according to the experimental observations [22], our simulations indicate that at the other damaged base pair, G10-C6, the base pairing is completely lost about 15% of the simulations time and at least one hydrogen bond is present about 85% of the simulations time [60].

Comprehensive descriptions of the different binding modes, as well as of the conformational and structural differences at the MutSα binding site (regarding both mismatch recognition and signaling subunits) and at the MutSα-DNA interface in response to damaged DNA recognition from the simulations herein are presented elsewhere [26, 60]. Here, a figure of the superimposed aligned representative structures for the mismatched and damaged MutSα-DNA recognition complexes is included in Online resource 4, Fig. 1. It provides a global view of the DNA conformational changes induced by the Pt-DNA adducts, as well as of the conformational changes within the mismatch recognition subunit, Msh6, and the signaling subunit, Msh2, in response to damaged or mismatched DNA recognition at the binding site and beyond.

Conclusions

We provide evidence indicating that strong, specific interactions at MutSα's protein-protein interface in response to the mismatched DNA recognition are replaced by weak, non-specific van der Waals interactions in response to the damaged DNA recognition, suggesting a severe impairment of the MutSα's dimerization in response to the damaged DNA recognition.

By comparison with the "default" mismatched DNA recognition, the MutSα's core is indicated as preserved in

response to the damaged DNA recognition. However, the loss of contact surface and the rearrangement of contacts at the protein-protein interface suggest a different packing in response to the "altered" damaged DNA recognition.

We predict that point mutations studies of the residues indicated to differentiate the MutSα's protein-protein interface in the repair versus cell-death conformations, namely residues 338, 391, 837, 869, and 947 of Msh6 and 721, 733, and 844 of Msh2, may allow the discovery of small ligands that would selectively induce these conformations, leading to new anticancer therapies targeting the MMR-dependent apoptotic pathway.

Correlated in the mismatched DNA recognition complex, interaction energies, hydrogen bonding, salt bridges, and solvent accessible surface areas become un-correlated or anti-correlated in response to the damaged DNA recognition. These pieces of evidence suggest that the loss of a synchronous mode of response while "surveying" post-replicative DNA would possibly be one of the cellular mechanism(s) of signaling the MMR-dependent programed cell-death much wanted in anticancer therapies.

Acknowledgments This research was partially supported by National Institute of Health R01CA129373 grand to FRS. The computational herein were performed on the Wake Forest University DEAC cluster. We thank Wake Forest University's Provost's office and Information Systems Department for their generous support.

References

1. Kunkel TA (1992) DNA replication fidelity. J Biol Chem 267: 18251–18254
2. Iyer RR, Pluciennik A, Burdett V, Modrich PL (2006) DNA mismatch repair: functions and mechanisms. Chem Rev 106:302–323
3. Peltomaki P (2003) Role of DNA mismatch repair deffects in the pathogenesis of human cancer. J Clin Oncol 21:1174–1179
4. Wang D, Lippard SJ (2005) Cellular processing of platinum anticancer drugs. Nature 4:307–321
5. Vasilyeva A, Clodfelter JE, Reactor B, Hills T, Scarpinato KD, Salsbury FR Jr (2009) Small molecule induction of Msh2-dependent cell death suggests a vital role of mismatch repair proteins in cell death. DNA Repair 8:103–113
6. Salsbury FR Jr, Clodfelter JE, Gentry MB, Hollis T, Scarpinato Drotschman K (2006) The molecular mechanism of DNA damage recognition by MutS homologs and its consequences for cell death response. Nucleic Acids Res 34:2173–2185
7. Vasilyeva A, Clodfelter JE, Gorczynski MJ, Gerardi AR, King SB et al. (2010) Parameters of reserpine analogs that induce MSH2/MSH6-dependent cytotoxic response. J Nucleic Acids. doi:10.4061/2010/162018
8. Fukui K, Shimada A, Iino H, Masui R, Kuramitsu S (2011) Biochemical properties of MutL, a DNA mismatch repair endonuclease. In: Storici F (ed) DNA repair - on the pathways to fixing DNA damage and errors. In Tech. doi:10.5772/23758
9. Gupta S, Gellert M, Yang W (2012) Mechanism of mismatch recognition revealed by human MutSβ bound to unpaired DNA loops. Nat Struct Mol Biol 19:72–79
10. Qiu R, DeRocco VC, Harris C, Sharma A, Hingorani MM, Erie DA, Weninger KR (2012) Large conformational changes in MutS during DNA scanning, mismatch recognition and repair signaling. EMBO J 31:2528–2540
11. Duckett DR, Drummond JT, Alastair IH, Murchie AIH, Reardon JT et al. (1996) Human MutSalpha recognizes damaged DNA base pairs containing 0^6-methylguanine, 0^4-methylthymine, or the cisplatin-d(GpG) adduct. Proc Natl Acad Sci U S A 93:6443–6447
12. Mello JA, Acharya S, Fishel R, Essigmann JM (1996) The mismatch-repair protein hMSH2 binds selectively to DNA adducts of the anticancer drug cisplatin. Chem Biol 3:579–589
13. Jiricny J (2006) The multifaceted mismatch-repair system. Nat Rev Mol Cell Biol 7:335–346
14. Kelland L (2007) The resurgence of platinum-based cancer chemotherapy. Nature 7:573–584
15. Drotschmann K, Topping RP, Clodfelter JE, Salsbury FR Jr (2004) Mutations in the nucleotide-binding domain of MutS homologs uncouple cell death from cell survival. DNA Repair (Amst) 3:729–742
16. Harrap KR (1985) Preclinical studies identifying carboplatin as a viable cisplatin alternative. Cancer Treat Rev 12:21–33
17. Rosenberg B, Van Camp L, Krigas T (1965) Inhibition of cell division in Escherichia coli by electrolysis products from a platinum electrode. Nature 205:698–699
18. Wheate NJ, Walker S, Craig GE, Onun R (2010) The status of platinum anticancer drugs in the clinic and in clinical trials. Dalton Trans 39:813–827
19. Andrews P, Howell S (1990) Cellular pharmacology of cisplatin: perspectives on mechanisms of acquired resistance. Cancer Cells 2:35–43
20. Shirazi FH, Wong PTT, Goel R (2003) Interaction of cisplatin with cellular macromolecules: a fourier transform infrared spectroscopy study. Iran J Pharm Res 2:11–15
21. Takahara PM, Rosenzweig AC, Frederick CA, Lippard SJ (1995) Crystal structure of double-stranded DNA containing the major adduct of the anticancer drug cisplatin. Nature 377:649–652
22. Teuben JM, Bauer C, Wang AHJ, Reedijk J (1999) Solution structure of a DNA duplex containing a cis-diammineplatinum(II) 1,3-d(GTG) intrastrand cross-link, a major adduct in cells treated with the anticancer drug carboplatin. Biochemistry 38:12305–12312
23. Wolfe KC, Hastings WA, Dutta S, Long A, Shapiro BA et al. (2012) Multiscale modeling of double-helical DNA and RNA: a unification through lie groups. J Phys Chem B. doi:10.1021/jp2126015
24. Kartalou M, Essigmann JM (2001) Recognition of cisplatin adducts by cellular proteins. Mutat Res 478:1–21
25. Jamieson ER, Lippard SJ (1999) Structure, recognition, and processing of cisplatin-DNA adducts. Chem Rev 99:2467–2498
26. Negureanu L, Salsbury FR Jr (2012) Insights into protein-DNA interactions, stability and allosteric communications: a computational study of MutSα-DNA recognition complexes. J Biomol Struct Dyn 29:757–776
27. Negureanu L, Salsbury FR Jr (2012) The molecular origin of the MMR-dependent apoptosis pathway from dynamics analysis of MutSα-DNA complexes. J Biomol Struct Dyn 30:347–361
28. Warren JJ, Pohlhaus TJ, Changele A, Iyer RR, Modrich PL et al. (2007) Structure of the human MutS DNA lesion recognition complex. Mol Cell 26:579–592
29. Brooks B, Bruccoleri RE, Olafson BD, States DJ, Swaminatan S et al. (1983) CHARMM: a program for macromolecular energy, minimization, and dynamics calculations. J Comput Chem 4:187–217
30. Jorgensen WL, Chandrasekhar J, Madura JD, Impey RW, Klein ML (1983) Comparison of simple potential functions for simulated liquid water. J Chem Phys 79:926–935
31. Humphrey W, Dalke A, Schulten K (1996) VMD: visual molecular dynamics. J Mol Graphics 14:33–38
32. MacKerell DA Jr, Banavali N, Foloppe N (2001) Development and current status of the CHARMM force field for nucleic acids. Biopolymers 56(257–265)
33. MacKerell DA Jr, Bashford D, Bellot M, Dunbrack RL, Evanseck JD et al. (1998) All-atom empirical potential for molecular modeling and studies of proteins. J Phys Chem B 102:3586–3616

34. Scheeff ED, Briggs JM, Hawell SB (1999) Molecular modeling of the intrastrand guanine-guanine DNA adducts produced by cisplatin and oxaliplatin. Mol Pharmacol 56(633–643)
35. Salsbury FR Jr, Crowley MF, Brooks CL (2001) Modeling of the metallo-beta-lactamase from B-fragilis: structural and dynamic effects of inhibitor binding. Proteins 44:448–459
36. Knaggs MH, Salsbury Jr FR, Edgell MH, Fetrow JS (2007) Insights into correlated motions and long-range interactions in CheY derived from molecular dynamics simulations. Biophys J:2062–2079
37. Salsbury FR Jr (2010) Molecular dynamics simulations of protein dynamics and their relevance to drug discovery. Curr Opin Pharmacol 10:738–744
38. Berendsen HJC, Postma JPM, van Gunsteren WF, DiNola A, Haak JR (1984) Molecular dynamics with coupling to an external bath. J Chem Phys 81:3684–3690
39. Kale L, Skeel R, Bhandarkar M, Brunner R, Gursoy A et al. (1999) NAMD2: greater scalability for parallel molecular dynamics. J Comput Phys 15:1283–1312
40. van Gunsteren WF, Berendsen HJC (1977) Algorithms for macromolecular dynamics and constraint dynamics. Mol Phys 34(1311–1327)
41. Darden T, York D, Pedersen L (1993) Particle Mesh Ewald: an N Log(N) method for Ewald sums in large systems. J Chem Phys 98:10089–10092
42. Hunenberger P, Mark AE, van Gunsteren WF (1995) Fluctuation and cross-correlation analysis of protein motions observed in nanosecond molecular dynamics simulations. J Mol Biol 252:492–503
43. Caves LSD, Evanseck JD, Karplus M (1998) Locally accessible conformations of proteins: multiple molecular dynamics simulations of crambin. Protein Sci 7:649–666
44. Straub JE, Rashkin AB, Thirumalai D (1994) Dynamics in rugged energy landscapes with applications to the S-peptide and ribonuclease. J Am Chem Soc 116:2049–2063
45. Horita DA, Zhang W, Smithgall TE, Gmeiner WH, Byrd RA (2000) Dynamics of the Hck-SH3 domain: comparison of experiment with multiple molecular dynamics simulations. Protein Sci 9:95–103
46. Auffinger P, Westhof E (1997) Three ns of multiple molecular dynamics simulations of solvated tRNA(ASP) anticodon hairpin. J Mol Biol 269:326–341
47. Salsbury FR Jr, Crowder MW, Kingsmore SF, Huntley JJA (2009) Molecular dynamics simulations of the metallo-beta-lactamase from Bacteroides fragilis in the presence and absence of a tight-binding inhibitor. J Mol Model 15:133–145
48. Loccisano AE, Acevedo O, DeChancie J, Schulze BG, Evanseck JD (2004) Enhanced sampling by multiple molecular dynamics trajectories: carbonmonoxy myoglobin 10 micros A0–>A(1–3 transition from ten 400 picosecond simulations. J Mol Model 22:369–376
49. Steinbach P, Brooks BR (1994) New spherical-cutoff methods for long-range forces in macromolecular simulations. J Comp Chem 15: 667–683
50. Lee B, Richards FM (1971) The interpretation of protein structures: estimation of static accessibility. J Mol Biol 55:379–400
51. Chothia C (1976) The nature of the accessible and buried surfaces in proteins. J Mol Biol 105:1–14
52. Raschke TM, Tsai J, Levitt M (2001) Quantification of the hydrophobic interaction by simulations of the aggregation of small hydrophobic solutes in water. Proc Natl Acad Sci U S A 98:5965–5969
53. Taylor A, Kennard O (1982) Crystallographic evidence for the existence of C–H–O, C–H–N and C–H Cl hydrogen bonds. J Am Chem Soc 104(5063–5070)
54. Desiraju GR, Steiner T (1999) The weak hydrogen bond in structural chemistry and biology. Oxford University Press, New York
55. Jeffrey GA, Saenger W (1991) Hydrogen bonding in biological structures. Springer Verlag, Berlin
56. Panigrahi SK, Desiraju GR (2007) Strong and weak hydrogen bonds in the protein-ligand interface. Proteins 67:128–142
57. Barlow D, Thornton JM (1983) Ion-pairs in proteins. J Mol Biol 168: 867–885
58. Karpen M, Tobias DJ, Brooks CL (1993) Statistical clustering techniques for the analysis of long molecular dynamics trajectories: analysis of 2.2-ns trajectories of YPGDV. Biochemistry 32:412–420
59. Matlab (2010) 7.10.0 edn. The MathWorks Inc., Natick, MA
60. Negureanu L, Salsbury FR Jr (2013) Non-specificity and synergy at the binding site of the carboplatin-induced DNA adduct via molecular dynamics simulations of the MutSα-DNA recognition complex. J Biomol Struct Dyn. doi:10.1080/07391102.2013.799437